Investigation of Novel Factors of Plasmodesmata Formation That Is Crucial for Multicellularity in Land Plants

陸上植物の多細胞化の鍵を握る原形質連絡を作り出す新奇因子の発見とその分子機構の解明

A DISSERTATION

Submitted to the Graduate School of Life Science,

Hokkaido University

In partial fulfillment of the requirements for the degree of

DOCTOR OF PHILOSOPHY

By CHIYO JINNO

March 2024

Contents

General introduction 4

Chapter 1; Abscisic acid changes cell polarity and cell fate of protonema in the moss *Physcomitrium patens* 8

Abstract 8

Introduction 9

Material and methods 11

Results 12

Discussion 15

Figure legends 18

Chapter 2; Abscisic acid signaling controls primary plasmodesmata density in the moss *Physcomitrium patens* 20

Abstract 20

Introduction 21

Material and methods 24

Results 27

Discussion 34

Figure legends 38

Chapter 3; Contribution of GGB-ROP signaling to PD formation and its relationship with ABA signaling in the moss *Physcomitrium patens* 43

Abstract 43

Introduction 44

Material and methods 46

Results 50

Discussion 54

Figures legends 57

General discussion 61

Acknowledgments 64

References 65

General introduction

Multicellular organisms are thought to have evolved from unicellular organisms consisting of a single cell in ancient times and were born after an extremely significant turning point, "multicellularity," in the long history of life. The evolutionary process of "multicellularity" is assumed to have occurred many times independently in various lineages, including animals, fungi, land plants, brown algae, and others (Grosberg and Strathmann, 2007; Knoll, 2011; Wegner et al., 2023). Multicellularity has enabled the evolution of a variety of organisms by providing them with complex structures and functions that have been constrained in unicellular organisms (Staps et al., 2019).

Asymmetric cell division (ACD) serves as a pivotal mechanism driving cellular diversification in multicellular organisms. It constitutes a fundamental process in cellular differentiation, posing a central inquiry within developmental biology. During this process, cells establish a polarity pattern (cell polarity) through the asymmetric localization of various proteins in the initial stages, ultimately leading to the cleavage of the cell into two daughter cells with distinct functions. This phenomenon of cell polarity is ubiquitous across the spectrum of life, from unicellular organisms like bacteria and yeasts to multicellular entities such as mammals, insects and plants (Treuner-Lange and Søgaard-Andersen, 2014; Rappel and Edelstein-Keshet, 2017).

Further, in addition to properly regulating cell polarity, multicellularity requires the acquisition of mechanisms to properly regulate cell adhesion, cell-to-cell communication, cell differentiation, and so on (Grosberg and Strathmann, 2007). During evolution, animals, plants, fungi and others have developed diverse structures for cell-to-cell communication in the regulation of developmental processes (Bloemendal and Kück, 2013) (see Graphical overview, general introduction). In animals, gap junctions are well-known as symplasmic connections. They consist of hemichannels formed by connexin or innexin spanning the plasma membranes of adjacent cells. Whereas gap junctions allow for small molecule transport down to 1 kDa (Hervé and Derangeon, 2013), tunneling nanotubes have

been identified as another type of cell connections in a variety of cell types and reported to facilitate even organelle exchange (Rustom et al., 2004). These two common structures known for short- and long-distance cell-to-cell communication are gap junctions and tunneling nanotubes, respectively. Fungi also have developed specialized structures named septal pores which across in the center of the transverse cell walls (septa) and allow cell-to-cell communication through cytoplasmic flow (Steinberg et al., 2017). In the Ascomycota of fungi, these pores can be plugged by the peroxisome-derived, fungal-specific Woronin body after hyphal injury to prevent excessive loss of cytoplasm (Jedd and Chua, 2000). Membrane-lined symplasmic cell connections were also found in red algae, called pit connections. Pit connections are formed between two daughter cells during annular ingrowth of the septal wall. They also form diverse proteinaceous pit plugs and cap membrane which seal the pore (Lee, 1971). In land plants and some green algae, a distinct structure of cell-to-cell communication is known as plasmodesmata (PD) that penetrate cross wall which is cell wall between cells. The space between the desmotubules linking them to the smooth endoplasmic reticulum (ER) of the cells on both sides and the inner surface of the channel, composed of the plasma membrane, serves as the conduit for molecular transport, primarily between cells (McLean et al., 1997). PD have also been found in brown algae, but they do not have an ER desmotubule structure (Terauchi et al., 2015). Brown algae and plant PD are thought to have evolved independently of each other. However, it is a mystery how both have acquired PD.

In land plants, PD are dynamically regulated in number and shape by developmental stages, cell types, and environmental signals (Sager and Lee, 2014; Tilsner et al., 2016). Based on observations using transmission electron microscope (TEM), the most common hypothesis of PD formation is that the ER meshwork is trapped in the newly forming cell plate during cell division, and the plasma-membrane-lined holes maintained in that area become PD (Porter and Machado, 1960; López-Sáez et al., 1966; Hepler, 1982). However, since the lack of PD, which is critical for cell-to-cell

communication, is thought to be lethal, little is known about the molecular mechanisms of PD formation.

In my study, the importance of PD in the maintenance of the multicellular regime in land plants led me to hypothesize that the molecular mechanisms of PD formation and its regulation could be approached by analyzing cell types and mutants with disrupted multicellular body plan. Then, I used the moss *Physcomitrium patens* in my research, which shows a relatively simple multicellular body plan among land plants (Rensing et al., 2020). The protonemal tissue in the moss *P. patens* is composed of cells arranged in a single row (see Graphical overview). In land plants, the plant hormone abscisic acid (ABA) is known for its involvement in stress response (Khandelwal et al., 2010), leading to the formation of stress-resistant stem cells referred to as brood cells in the case of *P. patens* (Schnepf and Reinhard, 1997; Hiroguchi et al., 2022). The protonemal apical cells usually show a cylindrical cell morphology, but within a few days after ABA application, they form brood cells with rounded cell shape, thick cell walls, and disrupted cell polarity (Arif et al., 2019; Hiroguchi et al., 2022). In non-seed plants, spores are known as diaspore to spread their distribution, and brood cells are thought to function as diaspore for vegetative propagation and are characterized by less cell adhesion in some mosses (Schnepf and Reinhard, 1997; Arif et al., 2019).

In chapter 1 of my dissertation, I first investigated changes in the multicellular body plan of the protonemal cells during brood cell induction. I found that ABA suppresses apical cell elongation and cell polarity of the cytoskeleton and vacuole in protonemal cells. I also found that ABA delays cell cycle progression. Given the potential function of brood cells as diaspores (Arif et al., 2019), I hypothesized that a severe defect of cell-to-cell communication has occurred in brood cells. Therefore, in chapter 2, I focused on PD of brood cells and found that PD density was reduced in these cells. Then, I investigated which factors in the ABA signaling pathway are involved in the reduction of PD density and found that ABA core module and one downstream transcription factor, ABA-

INSENSITIVE 5, is important for the regulation of PD density.

In the process of my research, I also hypothesized that cell-to-cell communication and the multicellular body plan are closely related. Therefore, I thought that mutants showing cells separating each other and losing their multicellularity, as in brood cells, may have less PD. Then, in chapter 3, I focused on mutants of a small GTPase, Rho of plants (ROP) which is known to regulate cell polarity, and its related factors that have apparently lost multicellularity (Cheng et al., 2020; Bao et al., 2022). I revealed marked decrease of PD density in these mutants and thus, ROP and its regulatory factors are important for PD formation. Taken together, I propose a regulatory mechanism for PD formation and its density in *P. patens*.

Through these findings, I present novel ideas concerning the comprehensive system of cell polarity and cell-to-cell communication that are crucial for independently evolving multicellularity.

Chapter 1; Abscisic acid changes cell polarity and cell fate of protonema in the moss *Physcomitrium patens*

Abstract

Multicellular organisms strictly control cell number and cell fate using asymmetric cell division (ACD) and symmetric cell division (SCD) during development and in response to the environment stimuli. While these processes generate various cell types in multicellular organisms, the molecular mechanisms underlying each mode of division and their transition remain largely unknown in plants. This study investigated the molecular mechanisms of the transition from ACD to SCD induced by the phytohormone abscisic acid (ABA) in the moss *Physcomitrium patens*. The apical cell of *P. patens* protonema, functioning as a stem cell, typically undergoes ACD to elongate the protonema. ABA, synthesized in response to environmental stresses, triggers the formation of stress-resistant brood cells from cylindrical apical cells. Among time-lapse and temporal observation of protonemal apical cells and observation of cytoskeletal and vacuolar markers, I investigated protonemal apical growth, cell polarity of apical cells, and cell division frequency during brood cell induction. My findings suggest that ABA suppresses apical growth, cell polarity, and the cell cycle. These alterations may hinder ACD while promoting SCD. Furthermore, my study highlights the pivotal role of SNF1-related protein kinase 2 (SnRK2) in the ABA-mediated inhibition of the cell cycle progression.

Introduction

Asymmetric cell division (ACD) is a fundamental mechanism driving cell diversification in multicellular organisms. In ACD, cells establish a polarity pattern by asymmetrically localizing various proteins, ultimately giving rise to daughter cells with distinct functions. In contrast, symmetric cell division (SCD) yields daughter cells of comparable shape, size, and fate (Tajbakhsh et al., 2009). Analysis and understanding of stem cells in land plants are important because stem cells determine the size of the general cell population and thus influence plant growth. However, the examination of stem cells in flowering plants is difficult due to their intricate presence within complex multicellular meristematic tissues. Consequently, the question of how stem cell division modes undergo transitions during development and how such modes are spatiotemporally regulated in response to varying environmental conditions persists as substantial challenges.

Within the protonema of the moss *Physcomitrium patens* (formerly recognized as *Physcomitrella patens*), conspicuous apical stem cells are readily observable (Kofuji and Hasebe, 2014). These cells show tip growth and undergo ACD, which is a typical stem cell feature (Yi and Goshima, 2020). In some moss protonemata, abiotic stresses such as low temperature, drought, and salt stress, as well as external application of the phytohormone abscisic acid (ABA), are known to suppress their growth and convert their cell fate to that of brood cells, which are stress-resistant cells (Schnepf and Reinhard, 1997; Zhao et al., 2018a). In a previous study, we showed that the application of ABA to the protonema of *P. patens* switched the cell division mode from asymmetric to symmetric (Hiroguchi et al., 2022). However, it is not fully understood what morphological changes occur in the cells during the switch in cell division mode from ACD to SCD and how stem cell activity is altered.

In this study, I examined changes in protonemal apical growth, apical cell polarity, and cell division frequency during the switch from ACD to SCD. The findings posit that ABA represses apical growth, cell polarity, and the cell cycle by modifying cytoskeletal and vacuolar function. These

alterations likely contribute to the inhibition of ACD while concurrently promoting SCD. Furthermore, the results propose that SNF1-related protein kinase 2 (SnRK2), a constituent of the ABA core module, assumes a pivotal role in growth inhibition and acquiring stress resistance during the brood cell induction process.

Material and methods

Plant materials and growth conditions

P. patens (Hedw.) Bruch & Schimp ssp. patens Tan strain was used as the wild type in this study (Nishiyama, 2000). *ProEF1α:D2* (as indicated by WT), *ProEF1α:D2/ppsnrk2qko* (*snrk2qko*) and *ProEF1α:D2/ppabi3tko* (*abi3tko*) lines were described previously (Kitagawa and Fujita, 2013; Tomoi et al., 2020). The plants were cultured on BCDAT medium with 0.8% (w/v) agar (Nacalai Tesque) under continuous white light at 25 ℃ (Nishiyama, 2000). GFP-Tubulin (Hiwatashi et al., 2008) and LifeAct-Venus (Era et al., 2009) were used as cytoskeleton markers. GFP-AtVam3 was used as a vacuole marker (Oda et al., 2009). For all experiments, protonema cells were embedded in 800 μL BCD with 0.8% (w/v) agar or BCDATG with 0.5% (w/v) gellan gum (Wako) instead of agar in 35 mm Petri dishes with a 27-mm coverslip window at the bottom (Iwaki). After inoculation, protonemal cells were cultured for 7 days under white light. To apply ABA to protonemal cells for live imaging, BCDATG liquid medium containing ABA (500 μM) or 1% (v/v) DMSO was added so that the final concentrations were 50 μM and 0.1%, respectively.

Microscopy

Tip growth and cell cycle progression were observed with an inverted microscope (ECLIPSE Ti-E, Nikon). Cytoskeleton markers and a vacuole marker were observed with an inverted microscope (ECLIPSE Ti2, Nikon) equipped with a spinning disk head (X light V3, CrestOptics) with a 1.40 NA 60× oil immersion objective (CrestOptics). Illumination with 470-nm and 520-nm laser light Emission filters were 510/50 nm for GFP and 560/40 nm for Venus. Image acquisition was controlled by MetaMorph (Molecular Devices). All images were processed using Fiji (Schindelin et al., 2012).

Results

ABA suppresses apical stem cell division and growth in an SnRK2-dependent manner

It has been reported that while ABA enhances stress tolerance in the protonemata of *P. patens*, it concurrently impedes its growth (Thelander et al., 2005). However, the direct association between ABA and cell division remains inadequately understood. Initial examination of apical cell growth under mock (DMSO) and 50 μM ABA treatments revealed the timescale at which ABA inhibits the growth of protonemal apical cells (Figure 1). After 1.5 hours, ABA-treated apical cells ceased elongating, displaying a rounded structure compared to the same cells at 0 hours.

In my observations of protonemata following ABA treatment, I observed that apical cells of the wild type (WT) protonema normally divide less than 10 hours, while apical stem cells hardly divide after ABA treatment (Figure 2A). Next, I investigated whether SnRK2 kinase, which functions centrally in ABA signaling, and ABI3, a transcription factor regulated by both SnRK2-dependent and SnRK2-independent manners (Zhao et al., 2018a; Komatsu et al., 2020), are involved in the regulation of cell division by ABA. For this purpose, I used the already established *snrk2* quadruple knockout mutant lacking *PpSnRK2A*, *B*, *C* and *D* genes (*snrk2qko*) and *abi3* triple knockout mutant lacking *PpABI3A*, *B* and *C* genes (*abi3tko*)(Khandelwal et al., 2010; Shinozawa et al., 2019; Tomoi et al., 2020), and compared the ratio of apical cells that had undergone cell division 72 hours after the start of ABA treatment. Mock treatment showed no difference between WT (gray circle) and both *snrk2qko* (orange diamond) and *abi3tko* (blue triangle) (Figure 2B). Conversely, under 50 μM ABA treatment, the ratio of apical cells that divided in WT and *abi3tko* was less than 20%, whereas *snrk2qko* (orange diamond) showed no reduction in the cell division rate (Figure 2C). This suggests that the suppression of cell division by ABA, and thus of cell cycle progression, is regulated by SnRK2 and not by ABI3.

Then, I examined the changes in the cell cycle progression during the formation of brood cells, which are induced a few days after ABA treatment. As showed in Figure 2A, the shape of WT

protonemal cells changed from cylindrical to a more swollen cell shaped brood cells within 72 hours of ABA treatment, accompanied by a reduction in chloroplast size and an increase in their number. Notably, both WT and *abi3tko* also dramatically slowed cell division up to 24 hours after the start of ABA treatment, but then all apical cells observed resumed cell division, even at a slower rate, and by 72 hours almost all cells had divided (Figure 2D). These results suggest that ABA treatment inhibits cell cycle progression under 24 hours treatment and regulates cell division at a slower rate than the normal cell cycle progression thereafter.

Asymmetries in the cytoskeleton and vacuole are disrupted in ABA-treated apical cells

While it is now evident that ABA is involved in the inhibition of cell cycle progression via SnRK2 kinase, the morphological changes at the cellular level remain elusive. Given the crucial role of the cytoskeleton in ACD, I examined the distributions of cytoskeletal components using GFP-Tubulin for tubulin (Hiwatashi et al., 2008) and LifeAct-Venus for actin (Era et al., 2009). In mock treatment and 0 hours of ABA treatment, tubulin and actin localized near the apical tip, as indicated by the white arrows in Figure 3A. However, at 3 hours of ABA treatment, no strong localization near the apical tip, as seen at 0 hours, was observed thereafter (Figure 3A). As the localization of microtubule and actin near the apical region is crucial for apical growth (Hiwatashi et al., 2014; Wu and Bezanilla, 2018), my results suggest that the ABA-induced reduction in apical growth is partially caused by the disruption of the apical tip localization of cytoskeletal components. Additionally, GFP-tubulin was used to observe spindle formation, a critical step in ACD (Leader et al., 2002; Yamada and Goshima, 2017). Under mock-treated conditions, I observed a prospindle (prophase spindle) at 0 minutes showing microtubule asymmetry, with strong fluorescence accumulation at the apical side (pointed by a red arrowhead), and a mitotic spindle (metaphase spindle) at 10 minutes (Figure 3B, DMSO). On the other hand, symmetric mitotic spindle formation was observed in ABA treatment (Figure 3B, ABA

at 0 minutes). Thus, my results suggest that ABA disrupts spindle asymmetry in brood cells.

My observation of the inhibition of apical cell growth led me to analyze the vacuole since an economical way for cell elongation is an enlargement of vacuoles (Krüger and Schumacher, 2018). Therefore, I analyzed the effect of ABA on vacuole shape using a GFP-AtVAM3 overexpression line as a vacuole maker (Oda et al., 2009). In the mock treatment, a large vacuole was observed on the basal side of the apical stem cell, whereas tubular vacuole structures were observed on the apical side (Figure 3C). However, this vacuolar asymmetry gradually lost during ABA treatment, with a significant change observed after 5 hours. Even the relatively large vacuoles on the basal side of the apical cell and in the sub-apical cell became finely fragmented and distributed evenly throughout the cell (Figure 3C). Thus, my findings regarding cytoskeleton, spindle morphology, and vacuole size and distribution support the idea that ABA broadly attenuates phenomena related to cell polarity, explaining the inhibition of apical stem cell growth.

Discussion

ABA core module regulates apical stem cell growth and cell division

The ABA core module, consisting of PYR/PYL/RCAR ABA receptors, PP2C phosphatase, and SnRK2 kinase, orchestrates direct phosphorylation of various transcription factors such as ABF (ABA-responsive element-binding factors) and ABI5 (Furihata et al., 2006). Additionally, transcription factors like ABI3 contribute to the ABA signaling pathway through their interaction with ABI5 (Skubacz et al., 2016). In this context, I demonstrated that the suppression of apical cell growth by ABA is mediated through SnRK2, a crucial component of the ABA core modules. While WT and *abi3tko* exhibit delayed cell cycle progression in an ABA-dependent manner, *snrk2qko* maintains cell division rates comparable to WT under mock treatment even in the presence of ABA (Figure 2B, C). Both WT and *abi3tko* display similar behaviors at all time points during 50 µM ABA treatment, exhibiting a significantly decelerated cell division rate without complete arrest (Figure 2D). ABA inhibits protonemal apical cell growth within 1.5 hours (Thelander et al., 2005) (Figure 1), whereas *snrk2qko* does not exhibit inhibition of apical cell growth even at high ABA concentrations of 50 or 100 µM (Shinozawa et al., 2019; Tomoi et al., 2020). Collectively, these findings suggest that SnRK2 regulates apical cell growth and the cell cycle progression, likely through the phosphorylation of its targets in an ABA-dependent manner.

The shift from ACD to SCD correlates with the loss of cell polarity in vacuolar and cytoskeletal distribution

Having identified the key signaling component responsible for ABA-dependent cell growth inhibition, the focus of this investigation now turns to understanding the cellular morphological changes occurring in protonemal cells. Apical cells, critical for stem cell function through ACD and apical growth, maintain polar elongation through polar secretion based on vesicular transport—a

phenomenon well-established in tip-growing cells such as pollen tubes (Yong et al., 2008; Wang et al., 2013a). This observation aligns with my data and previous findings in apical cells of *P. patens*, indicating the polar localization of actin and tubulin at the apical tip (Hiwatashi et al., 2008; Wu and Bezanilla, 2018). In my study, both arrest of apical growth and loss of cytoskeletal polar localization were observed within 3 hours of ABA treatment (Figure 1 and Figure 3A), suggesting that the effect of ABA on the cytoskeleton is likely responsible for the inhibition of apical cell elongation.

Another significant factor during cell growth, particularly elongation, is the plant vacuole (Dünser et al., 2019). The vacuole is a cell organelle that responds to its environment (Krüger and Schumacher, 2018) and the expansion of the vacuole promotes rapid cell growth. This is corroborated by my data (Figure 3C), where, in the absence of ABA, large vacuoles are evident on the basal side of the apical cell, reducing the energetic cost of cell elongation. In contrast, tubular vacuolar structures dominate the apical side of the apical cell. However, upon ABA application, this asymmetry dissolves, and tubular vacuolar structures and smaller vacuoles distribute evenly throughout the cell (Figure 3C). And in brood cells, a loss of large vacuoles is observed (Schnepf and Reinhard, 1997; Arif et al., 2019). After ABA application, the apical cells of protonema are rounded at the tip and swollen overall, including the sides of the cell (Figure 2A). These results suggest that ABA-induced changes in vacuolar morphology from the large vacuole to smaller vacuolar structures affect the change in growth direction of protonemal cells from anisotropic to isotropic growth, which may lead to the suppression of apical cell elongation.

An additional cellular physiological observation pertains to the spindle. In terrestrial plant species, spindles observed during the ACD process have been documented in the zygotes or germinating spores of *Marchantia polymorpha* (Ueda et al., 2011; Sakai et al., 2022). Within the germinating spores of *M. polymorpha*, there is an uneven localization of microtubules at the initiation of prospindle formation, and ACD is observed after the movement of prospindle in the direction of this microtubule

accumulation (Sakai et al., 2022). This implies that the accumulation of microtubules in the migratory direction plays a pivotal role in the migration of the prospindle or nucleus. In *P. patens*, I observed microtubule accumulation in the prospindle was noted in apical protonemal cells under mock treatment, indicative of apical growth (Figure 3B). Given that ABA suppresses the apical growth of cells (Fig. 1A), it is predicted that ABA may also suppress the apical migration of nuclei by mitigating microtubule bias in the prospindle.

Taken together, these observations of the loss of asymmetry in the distribution of actin, tubulin, vacuoles, and spindle structures indicate a loss of cell polarity in apical stem cells under ABA treatment. Tip growth is maintained by the apical localization of tubulin and actin, potentially implicated in vesicular trafficking to tip region of the apical cell. Enlarged vacuoles on the basal side of the apical cell reduce the energy expenditure associated with cell elongation, while the apical side with its tubular vacuolar structure contains a large cytoplasmic volume, which can accommodate the volume requirements of the phragmoplast and its associated cell plate-forming structures (Seguí-Simarro and Staehelin, 2006). Thus, ABA plays a role in the disruption of cell polarity, which in turn induces isotropic cell elongation and the transition to SCD. The loss of intracellular asymmetry aligns seamlessly with the shift in cell morphology of protonemal cells, transitioning from cylindrical to a more swollen and rounded configuration (Figure 2A), suggesting that ABA is involved in the transition from anisotropic apical growth to isotropic diffuse growth.

Figure legends

Figure 1: Tip growth is suppressed immediately upon ABA treatment. Time-lapse imaging of tip growth in 0.1% DMSO as a mock treatment (left) and 50 μM ABA treatment (right). 0 h indicates the start of treatment. The apical cell continued to elongate with mock treatment, but with ABA treatment, it stopped elongating after 1.5 hours and its apical apex became round, as indicated by a white arrow. Micrographs indicate the respective time course of 1 exemplary cell. Each treatment was carried out with n = 5-8. Black lines indicate the same X-axis position. Scale bar = 20 μm.

Figure 2: ABA suppresses cell cycle progression via SnRK2, not by ABI3. (A) Morphological change of protonemal cells during 50 μM ABA treatment for 72 hours. The treatment duration is shown in each micrograph. Cells were observed from 1 h after reagent treatment (t=0). Scale bar = 20 μm. **(B), (C)** Cell division ratio of protonema apical cells in a time course under DMSO treatment or ABA treatment. WT (gray circle), *snrk2qko* (orange diamond) and *abi3tko* (blue triangle) were observed from 1 h after reagent treatment (t=0), and the percentage of apical cells passing the M phase was determined at each time interval. Each point is shown as the mean ± SD of 3 independent experiments with n=10-20 each. **(D)** Cell division ratio of protonema apical cells in a time course. WT and *abi3tko* were observed from 1 h after reagent treatment (t=0), and the percentage of apical cells passing the M phase was determined at each time interval. Each point is shown as the mean ± SD of 3 independent experiments with n =10-20 each.

Figure 3: ABA suppress microtubule and actin localization on the apical apex, and vacuolar asymmetry. (A) Fluorescence images of protonema apical cells expressing GFP-Tubulin and LifeAct-Venus that were treated with 0.1% DMSO or 50 μM ABA. Images were taken immediately (0 h, left) and 3 hours (right) after the reagent treatment. White arrows indicate the fluorescence accumulation

at the apical apex. 5-8 independent apical cells were observed in each condition with a confocal microscope. **(B)** Time-lapse images of GFP-Tubulin in the cell division zone treated with 0.1% DMSO or 50 μM ABA. In the DMSO treatment, GFP-Tubulin fluorescence accumulated on the apical side pointed by a red arrowhead in the early stage of spindle formation. The direction of the white arrows is apical side of protonema. In ABA treatment, the fluorescence polarity disappeared from the early stage of cell division. n = 2-5. Scale bar = 10 μm. **(C)** Fluorescence images of apical cells expressing GFP-AtVam3 that were treated with 0.1% DMSO or 50 μM ABA. The treatment duration is shown in each micrograph. White arrows indicate cross walls between apical cells and subapical cells. The micrographs represent one exemplary sample, one for DMSO and one for the ABA time course. Scale bar = 20 μm.

Chapter 2; Abscisic acid signaling controls primary plasmodesmata density in the moss *Physcomitrium patens*

Abstract

Plasmodesmata (PD), specialized nanostructures exclusive to land plants, intricately orchestrate cellular communication, growth, and stress resilience, thereby contributing significantly to overall the plant survival. While the role of callose in modulating PD permeability is well-documented, the regulatory mechanisms dictating PD number and structure, particularly their evolutionary origins, remain elusive. Here I demonstrate that abscisic acid (ABA), which induces the formation of stress-resistant diaspores in the moss *Physcomitrium patens*, reduces PD density in this cell population. The ABA core module and a downstream transcription factor, ABA INSENSITIVE 5 (ABI5), are crucial for the regulation of PD density. This observation underscores the regulation of cell-to-cell communication through the suppression of primary PD formation, which is induced by ABA signaling. Since ABA signaling pathway has established in the progenitors of land plants, it has potentially played a crucial role in their adaptation to challenging terrestrial environments.

Introduction

The regulation of cell-to-cell communication is essential for the growth and environmental responses of multicellular organisms. Animals use connexin, which is a well-established factor in the formation and regulation of gap junctions for cell-to-cell communication and cell adhesion (Söhl and Willecke, 2004). Changes in connexin expression and localization affect on cell proliferation, migration, and tumor growth (Wu and Wang, 2019). In contrast, land plants, another major group of multicellular organisms, have developed symplasmic cell connections for cell-to-cell communication, called plasmodesmata (PD) (Cilia and Jackson, 2004). PD are present in extant lineages of the Charophyte alga orders Charales and Coleochaetales, as well as all land plants, and are believed to have originated from the common ancestor of current Phragmoplastophyta species, which form a phragmoplast during a cell division (Bowman, 2022).

Most research on cell-to-cell communication via PD has been conducted in angiosperm species. These studies have revealed variations in both PD density and structure across distinct cell types, with modifications occurring at diverse developmental stages and in response to environmental stress (Burch-Smith et al., 2011; Sager and Lee, 2014). The most common hypothesis during PD formation (based on electron microscopy) is that the endoplasmic reticulum meshwork is trapped in the newly forming cell plate during cell division, and the plasma-membrane-lined holes maintained in that area become primary PD (Porter and Machado, 1960; López-Sáez et al., 1966; Hepler, 1982). However, the molecular mechanisms of primary PD formation, the regulation of PD number in the cell plate, and the control of PD formation in different cell contexts in various environments are poorly understood (Nicolas et al., 2017). Secondary PD are also formed *de novo* in existing cell walls between cells (cross walls). In *Arabidopsis thaliana*, secondary PD formation is positively regulated by the seven-bladed WD40-repeat protein DSE1 (Xu et al., 2012) and the choline transporter CHER1 (Kraner et al., 2017) and is negatively regulated by signals controlled by the organellar RNA helicases ISE1

and ISE2 (Burch-Smith and Zambryski, 2010). Notably, the impact of these factors on secondary PD formation is presumed to be indirect, as none of these factors localizes directly to PD (Sager and Lee, 2018).

Recent studies have uncovered another layer of regulation of cell-to-cell communication via PD. The transient and reversible modulation of PD permeability during development and stress responses through callose deposition has been unveiled (Zavaliev et al., 2011). Callose deposition appears at primary PD in newly formed cell walls; after cell division, callose is often found at PD neck regions (Radford et al., 1998). Alterations in callose levels at PD are instigated by beta-1,3-glucanases or beta-1,3-glucan synthases; plants deficient in these enzymes undergo modifications in the upper limit of the size of molecules permeating through PD, defining the size exclusion limit of PD (Levy et al., 2007; Vatén et al., 2011). Diverse studies have described the regulation of callose deposition onto PD through pathways reliant on reactive oxygen species, auxin, abscisic acid (ABA), or salicylic acid (Han et al., 2014; Sager and Lee, 2014; Tylewicz et al., 2018; Sankoh and Burch-Smith, 2021). Thus, callose-dependent PD permeability regulation in different contexts of developmental decisions and environmental stress has been gradually uncovered in angiosperms.

In contrast to studies of PD in angiosperms, limited research has been documented regarding Charophyte algae and non-vascular plants. We recently found that PD permeability decreases in the filamentous protonemata tissue of the moss *Physcomitrium patens* without changes to PD density within 1 h after ABA treatment (Kitagawa et al., 2019). This regulation occurs via the core components of ABA signaling, including the protein kinase SUCROSE NONFERMENTING 1-RELATED PROTEIN KINASE 2 (SnRK2), the type 2C protein phosphatase ABA-INSENSITIVE 1 (ABI1), and the downstream factor ABA-INSENSITIVE 3 (ABI3), a B3-type transcription factor, partially (Tomoi et al., 2020). These findings underscore the significance of a conserved ABA-dependent signaling pathway in both mosses and flowering plants, potentially governing cell-to-cell communication via

PD (Kitagawa and Fujita, 2015; Kitagawa et al., 2019; Tomoi et al., 2020). Conversely, this rapid (< 1 hour) suppression of PD permeability in moss appears to operate independently of callose, suggesting that PD regulation might be more elaborately fine-tuned to developmental stages and environmental conditions (Kitagawa and Fujita, 2015; Kitagawa et al., 2019; Tomoi et al., 2020). In *P. patens*, extended ABA treatment or exposure to environmental stress transforms normal protonemal cells into specialized stress-resistant stem cells termed brood cells (Arif et al., 2019; Hiroguchi et al., 2022). Cell-to-cell communication was drastically suppressed among these cells, as we could not detect any movement of a fluorescent protein from a cell to the neighboring cells over more than 2 days of observation (Kitagawa and Fujita, 2015).

Here, I investigated PD density and structure in the cross walls of brood cells under long-term (> 4 days) exposure to ABA or osmotic stress. I discovered that ABA reduced the primary PD number per cell wall in brood cells and that ABA core module components, Pyrabactin resistance/Pyrabactin resistance-like/Regulatory component of ABA receptor (PYR/PYL/RCAR-type-ABA receptor), ABI1 and SnRK2, are all essential for this regulation. Moreover, a well-conserved transcriptional factor in ABA signaling pathway in land plants, ABA-INSENSITIVE 5 (ABI5) but not ABI3 plays a pivotal role on PD formation. Thus, my study unveils a new pathway for the role of environmental stress in regulating primary PD density. This might also represent an important survival strategy for the adaptation of ancestral land plants to the terrestrial environment.

Material and methods

Plant materials and growth conditions

The moss *Physcomitrium patens* (Hedw., formerly *Physcomitrella patens*) Bruch & Schimp accession Gransden was used in this study as the wild type. The *ProEF1α :D2* and *Ppsnrk2qko* lines in the *ProEF1α:D2* background (*snrk2qKO*), *Ppabi3tko* in the *ProEF1α:D2* background (*abi3tKO*), *PpSnRK2AiOX* in the *ProEF1α:D2* background (*SnRK2iox*), and *PpABI3AiOX* in the *ProEF1α:D2* background (*ABI3iox*) were previously described (Kitagawa and Fujita, 2013; Tomoi et al., 2020). *PpABI1A^{G333D} OX/ProEF1α:D2*, which was used as the overexpression line of the dominant negative form of *ABI1*, was described previously (Tomoi et al., 2020). The GFP-tubulin line was used as a tubulin marker (Hiwatashi et al., 2008). All plants were subcultured on BCDAT medium solidified with 0.8% (w/v) agar (Nacalai Tesque) under continuous white light (30 μmol m^{-2} s^{-1}) at 25°C (Nishiyama, 2000).

Treatment and observation of protonemata

Protonemal tissues were prepared in glass-bottom dishes (four-well glass-bottom chamber; Iwaki) to enable detailed observations of the cross wall BCDATG (BCDAT and 0.5% [w/v] glucose) solidified with 0.8% agar (w/v) was used as culture medium. After the moss was transplanted to the bottom of the chamber, the chamber was turned upside down and incubated under continuous red light (20 μmol m^{-2} s^{-1}) for 5-7 d. The position of the septa was determined by the incubator. The position of the septa was checked under an inverted microscope (ECLIPSE Ti-E, Nikon) or an upright microscope (BX60, Orympus) before and 4 d after the administration of 0.1% (v/v) DMSO (mock treatment) or 50 μM A treatment) or 50 μM ABA.

To wash out the ABA, the glass-bottom chamber treated with ABA was submerged in 100 ml

liquid BCDATG medium for 24 h. The liquid medium was discarded, and the protonemata were observed. The culture was transferred to red light (20 μmol m^{-2} s^{-1}) and incubated for 4 d.

For mannitol treatment of the WT and ABA treatment of *snrk2qKO* and *abi3tKO*, mosses were grown in liquid BCDAT medium in 24-well plates for 5 d with continuous white light. Mannitol was applied at final concentrations of 0.1 and 0.3 M, and ABA was applied at a final concentration of 50 μM, followed by incubation for 4 d.

Transmission electron microscopy

Protonemal tissues were fixed in 3% (w/v) glutaraldehyde (Nisshin EM) and 1% (w/v) formaldehyde (freshly prepared from paraformaldehyde, TAAB) in 0. After rinsing in 0.1 M sodium phosphate buffer, the material was post-fixed with 1% (w/v) osmium tetroxide (Nisshin EM) in 0.1 M sodium phosphate buffer, pH 6.8, overnight at 4°C, dehydrated through an ethanol series, and embedded in Spurr resin (mixing ERL4221, DER736, NSA [Polysciences]). Sections were sequentially stained with EM Stainer (Nisshin EM) for 30 min, stained with lead stain solution (Sigma-Aldrich Japan) for 8 min, and examined under a H-7650 transmission electron microscope (Hitachi High-Tech).

Aniline blue staining

Aniline blue (Biosupplies) was dissolved in sterile water to 1 mg/ml and stored as a stock solution at 4°C in the dark. When glass-bottom chambers were used, fresh solutions were prepared by diluting the solution to 330 μg/ml in 100 mM phosphate buffer (pH 8.5) and used to treat samples for 1 d before observation at a final concentration of 33 μg/ml. Moss plantlets grown in liquid medium were picked out and placed in a fresh solution diluted to 33 μg/ml in 100 mM buffer (pH 8.5) and incubated at room temperature for 30 min. Aniline blue fluorescence was detected under a Zeiss LSM980 confocal microscope equipped with a Plan-Apochromat 63×/1.40 oil DIC M27 objective. A 405-nm

laser with 0.2% power intensity was used to excite aniline blue. The detection range was 410–605 nm. Fluorescence spot density was measured based on super resolution radial fluctuation (SRRF) images. NanoJ-SRRF (Gustafsson et al., 2016), a plug-in for ImageJ (Fiji), was used to obtain one SRRF image from 10 consecutive images. The number of spots was counted in ImageJ, and spot density was calculated based on the length of the area where aniline blue fluorescence was observed in the cross walls.

Phylogenetic analysis of PYR/PYL/RCAR ABA receptor

To make phylogenetic trees of PYR/PYL/RCAR receptors, alignment of full-length proteins was constructed using MUSCLE alignment (Edgar, 2004). A non-rooted maximum-likelihood phylogenetic tree was constructed using the LG as substitution model. Letters of branches denote bootstrap support based on 100 repetitions.

Quantification and statistical analysis

The density of aniline blue fluorescence spots on cross walls was quantified using Fiji-ImageJ. Statistical analyses were performed using R ver. 4.0.2. For the multiple sample comparison, one-way ANOVA with post-hoc Tukey HSD test was performed (Tukey, 1949). For two sample comparison, Welch's t-test was performed (Welch, 1938). Graphs were generated using the R ggplot2 package, BoxPlotR, or Microsoft Excel. The value of n indicates the number of samples. Statistical significance was set at $P < 0.01$.

Results

ABA decreases PD density in the newly formed cell walls of brood cells

Compared to clinder-shaped normal protonemal cells, brood cells show a rounded cell morphology with lost cell polarity (Figure 1A, white asterisks). Brood cell formation is fully induced after several days of ABA treatment (as a long-term treatment) in the range of 25-100 μM (Busch et al., 2013; Arif et al., 2019; Hiroguchi et al., 2022). Among these brood cells, we noticed that cell-to-cell communication was drastically suppressed (Kitagawa and Fujita, 2015). To investigate this further, I examined PD in cross walls of 50 μM ABA-treated protonema using transmission electron microscopy (TEM), revealing a reduction in PD numbers on the sections of cross walls in ABA-treated sample (Figure S1A). Subsequently, I explored whether this reduction in PD numbers occurred at pre-formed cross walls or newly formed cross walls during 4 d of ABA treatment. Distinguishing two types of cross walls within the same protonemal filament (Figure 1A, pre-formed cross walls pointed by blue arrows vs. newly formed cross walls pointed by yellow arrows), I observed PD in each type of cross walls by TEM (Figure 1B). There was no significant difference in PD density in cross walls of the mock-treated control and pre-formed cross walls before ABA application. However, PD density decreased by half (50.5% of the mean PD density) in cross walls that were newly formed after ABA application (Figure 1C, the mean PD density before vs. after treatment = 1.087/μm vs. 0.539/μm). These results suggest that prolonged ABA treatment reduces PD density in newly formed cross walls after ABA application and that at least within 4 days there is no secondary reduction in PD density of pre-formed cross walls. Notably, no PD with complex, branched structures were detected after long-term ABA treatment; all PD exhibited a simple structure (Figure S1B). Our previous study suggests that ABA reduces PD permeability by narrowing the PD aperture (Kitagawa et al., 2019), so I measured the width of the PD aperture in the pre-formed and newly formed cross walls in ABA treatment. As a result, a decrease in width was observed in both types of cross walls under ABA

treatment compared to mock (Figure S1C).

To ascertain whether PD density could be restored or maintained at lower levels in newly formed cross walls after ABA was removed, brood cells were transferred to an ABA-free environment, leading to the regeneration of normal protonemal cells through asymmetric cell division (Figure 1D). PD in the cross walls of these regenerated protonemal cells were examined (Figure 1E), revealing a recovery in PD density of newly formed cross walls after ABA removal to levels similar to those observed in mock treatment (Figure 1E and 1F, the mean PD density; treatment vs. removal = 0.336/μm vs. 0.736/μm). This indicates that the reduction in PD density during brood cell differentiation is transient and flexible, contingent upon the presence of exogenous ABA. To complement these findings, aniline blue staining, a standard method for assessing PD density (Tomoi et al., 2020; Muller et al., 2022), was performed to detect PD-associated callose accumulation (see Methods and Figure S1D). The observed decline in PD-associated callose density in newly formed cross walls after ABA treatment concurred with the results obtained through direct TEM observation of PD (Figure 1C and 1G). Notably, PD density values were higher in aniline blue staining than in TEM observation, likely due to better visualization of cell wall thickness in the staining method. When treated with different ABA concentrations ranging from 20 μM to 100 μM in aniline blue staining, the decreasing trend in PD density reached a plateau above 50 μM (Figure S1E).

ABA decreases primary PD number in newly forming cell plates of brood cells

While prolonged exposure to ABA led to a reduction in the PD density of newly formed cell walls, it remained uncertain whether this decrease resulted from a reduction in the number of primary PD formed during cell division or from subsequent secondary destruction of primary PD once established. To address this, I investigated whether the decline in PD density along cross walls of brood cells was linked to a block in primary PD formation occurring in newly forming cell plates or to the secondary

destruction of primary PD in cross walls. This analysis required the identification of newly forming cell plates during cytokinesis, which are rare in brood cells compared to normal protonemal cells since cell cycle progression is much slower in brood cells (Hiroguchi et al., 2022) (Chapter 1; Figure 2C). To achieve this, I examined a *P. patens* line expressing green fluorescent protein (GFP) tagged tubulin to help identify phragmoplasts, plant specific cylindrical structures consisting of microtubules and actin filaments. Given that primary PD can form during late cytokinesis (e.g., anaphase to telophase) when the phragmoplast is developing, analyzing this time frame enabled the examination of primary PD formation (Figure 2A). As observed in ultrathin sections, the newly forming cell plates (Figure 2B, cell plate) were thinner than fully developed mature cross walls (Figure 2B, cross wall) and showed larger-sized pores (Figure 2B, green arrows) in addition to PD-sized pores (Figure 2B, magenta arrowheads); both features were used as indicators of newly forming cell plates in brood cells.

As I could not predict whether larger-sized pores I found in the cell plates would develop into PD or become part of the cross wall by becoming filled with cell wall components, first I evaluated only the density of PD-sized pores in the cell plates. During the process of cytokinesis, an expanding cell plate is expected to gradually thicken and finally become a cross wall. Therefore, the thickness of the cell plate was used to evaluate the stage of the cell plate. I expected the PD-sized pore density to increase with increasing thickness in the cell plate, but contrary to my expectation, no correlation was found between cell plate thickness and PD-sized pore density in the cell plate in the mock and ABA treatment, respectively (Figure 2C, mock, $r = 0.1618$; ABA, $r = 0.1628$). This suggests that it is difficult to estimate the growth stage of the cell plate by its thickness. PD-sized pore density was significantly reduced in ABA compared to mock (mock vs. ABA = 0.583/μm vs. 0.176/μm; 69.8% reduction in mean density, $P < 0.01$). However, ABA may also affect the thickening of the cell plate since the cell plate in ABA treatment was more fragmented at similar thicknesses as mock (Figure 2B). Therefore, it is possible that the decrease in PD-sized pore density in ABA treatment is due to the

younger stage of the observed cell plates compared to those in mock treatment.

In addition, I compared the PD density and thickness of the cross walls under mock and ABA treatment. The thickness of cross walls was thicker in the ABA treatment than in mock (Figure 2C, black triangle v.s. dark yellow triangle). The density of combined PD-sized pores and larger-sized pores in the observed cell plates was not significantly different between mock and ABA (Figure 2D, all pores mock v.s. ABA). However, the decreased PD density in cross walls newly formed after ABA application compared to the mock (Figure 2D, PD mock v.s. ABA) suggests that under ABA treatment, the pores formed during cell division may be filled and no longer remain as PD.

ABA core module is crucial for the ABA-induced reduction of primary PD density

Recent studies have underscored the pivotal functions of the ABA core signaling pathway in abiotic stress, a mechanism likely established in the ancestors of bryophytes and consistently preserved across land plants (Cutler et al., 2010; Komatsu et al., 2020; Sun et al., 2020). We previously demonstrated that short-term (<3 hours) ABA or salt stress led to a reduction in PD permeability in *P. patens* protonemata, both in callose-independent and -dependent manners, and that this regulation requires the B3-type transcription ABI3 as well as SnRK2 and ABI1, the upstream kinase and phosphatase components of the ABA core module, respectively (Tomoi et al., 2020). Despite the unaffected PD density following short-term ABA treatment, I investigated whether ABI3, SnRK2, and ABI1 played a role in the reduction of PD density induced by long-term ABA treatment (>4 days) in brood cells. To address this, I examined the *Ppabi3* triple mutant (*abi3tKO*) (Khandelwal et al., 2010). Whereas *abi3tKO* showed similar growth and protonemal cells to the wild type (WT) before ABA treatment (Figure S2A), ABA-treated *abi3tKO* produced brood cells and displayed a lower PD density to the same degree as in the ABA-treated WT (Figure 3A and 3B). These findings imply that ABI3 does not contribute to the ABA-induced reduction in primary PD formation.

I then explored the involvement of SnRK2 by examining the impact of ABA treatment on the *Ppsnrk2* quadruple mutant (*snrk2qKO*) (Shinozawa et al., 2019). Same as the *abi3tKO* mutant, *snrk2qKO* showed similar growth and cell morphology in the protonemata to the WT under normal conditions (Figure S2A); however, ABA-treated *snrk2qKO* produced no brood cells and did not exhibit decreased PD density in newly formed cross walls after ABA application (Figure 3A and 3B). These findings underscore the critical roles of SnRK2 in both brood cell formation and the suppression of primary PD formation. In a complementary approach, I inducibly overexpressed *ABI3A* or *SnRK2A* (Tomoi et al., 2020) using an estradiol-inducible system (β-est). Overexpression of *ABI3A* had little effect on cell shape and no effect on PD density (Figure S2B and S2C). On the other hand, although overexpression of *SnRK2A* showed swollen cell morphology, there was no significant difference in PD density (Figure S2D and S2E). These results suggest that SnRK2 may be essential but not sufficient for the regulation of PD density by ABA.

I then examined the alterations in PD density in *ABI1* mutants. As ABI1 functions as a negative regulator of ABA signaling, the *abi1* double mutant (*abi1dKO*) (Komatsu et al., 2013) exhibited brood cells even in the absence of ABA treatment (Figure 3C). In contrast, an overexpression line of the dominant negative form of *ABI1A* (*abi1-DN*) (Tomoi et al., 2020), which is insensitive to ABA, displayed no brood cell formation even under 4 days of ABA treatment (Figure 3C). Consequently, *abi1dKO* exhibited a lower PD density even in mock condition, comparable to the reduction observed in ABA-treated WT (Figure 3D). Conversely, *abi1-DN* plants, insensitive to ABA, exhibited neither brood cell formation nor a reduction in PD density under ABA treatment. Taken together, these data suggests that ABI1 is implicated as a negative regulator in the regulation of PD density by ABA.

Two of the three components of the ABA core module, SnRK2 kinase and PP2C phosphatase (ABI1), were found to be responsible for primary PD formation. Thus, I further investigated whether the remaining ABA core component, the ABA receptor, is also involved in PD formation. The

PYR/PYL/RCAR-type-ABA receptor is well-conserved between *P. patens* and *A. thaliana*, and molecular phylogenetic analysis revealed that five orthologous receptors are present in the moss (named *pyl1*; *Pp3c9_19760*, *pyl2*; *Pp3c7_26290*, *pyl3*; *3c26_15240*, *pyl4*; *Pp3c13_7110* and *pyl5*; *3c3_660*) (Figure S3A). Assuming that the individual ABA receptors in the moss may function redundantly, as reported for many of them in *A. thaliana* (Park et al., 2009; Zhao et al., 2018b), I obtained two independent quadruple knock-out mutants (*pylqKO*), *pyl1234qKO* or *pyl1345qKO* mutant. Then, I examined their involvement in PD formation and found that both *pylqKO* mutants were insensitive to exogenous ABA and did not form brood cells under 4 days of ABA treatment (Figure 3E). The result suggests that these proteins act as bona fide ABA receptors in *P. patens*. More importantly, these mutants did not show the reduction of PD density even under ABA treatment (Figure 3F). Taken together, these data suggest that ABA core signaling modules is crucial for the ABA-induced reduction of primary PD density.

ABI5 functions as a downstream factor in the regulation of PD density by ABA

I demonstrated that the ABA core signaling module is crucial for the regulation of PD density, while one of the downstream transcription factors of the core signaling, ABI3, was not involved. Consequently, I sought another downstream factor that plays a significant role in PD density regulation. ABA-INSENSITIVE 5 (ABI5) is a leucine zipper-type transcription factor and a key substrate of SnRK2 in ABA responses in *A. thaliana* (Nakashima et al., 2009; Wang et al., 2013b). Additionally, it has been reported that a peptide fragment derived from ABI5 is phosphorylated by SnRK2 under ABA treatment (Shinozawa et al., 2019) . Therefore, ABI5 emerges as a promising candidate for the ABA signaling pathway in the regulation of PD density. A Blast search and phylogenetic analysis revealed the presence of three ABI5 orthologous genes (*Pp3c20_7230*, *Pp3c20_7290*, and *Pp3c23_19420*) in

the *P. patens* genome, named as *ABI5A*, *5B* and *5C*, respectively (from Sakata *et al*. (unpublished)). Then I obtained independent *abi5ab* double knockout mutants (*abi5dKO*), and they did not form brood cells under 4 days of ABA treatment (Figure 4A). Further, I examined PD density under ABA treatment and found that *abi5dKO* did not exhibit the reduction of PD density (Figure 4B), suggesting that ABI5A and 5B plays a crucial role in PD density regulation through ABA core signaling components in *P. patens*.

To further validate whether environmental stress, as well as exogenously supplied ABA, reduces PD density, I investigated the effects of abiotic stress. I chose osmotic stress, known to elevate endogenous ABA levels and activate a stress response mediated by SnRK2 in *P. patens* (Toriyama et al., 2022). I examined changes in PD density in protonemal cells exposed to osmotic stress and observed that treatment with 0.3 M mannitol, but not 0.1 M mannitol, induced the formation of brood cell-like swollen cells (Figure 4C), wherein PD density was reduced (Figure 4D). Due to the lethal effects of severe osmotic stress on mutants lacking ABA core components (Shinozawa et al., 2019) (Figure S4), I could not investigate PD density under osmotic stress conditions in this mutant. Nevertheless, these results suggest that environmental stress, possibly by increasing endogenous ABA levels and acting through the ABA core signaling pathway, hinders cell-to-cell communication by reducing PD density in cross walls (Figure 4E).

Discussion

In this study, I identified that ABA and its core signaling components exert a suppressive effect on primary PD density. This regulation is associated with a decrease in the density of pores maintained as PD in newly forming cell plates during cytokinesis, and interestingly, this effect persists, maintaining low PD density even in mature cross-walls (Figure 2). Notably, the roles of stress or phytohormones in influencing primary PD density have not been previously reported. While cytokinins and salicylic acid have been recognized to promote PD formation in angiosperms (Ormenese et al., 2006; Fitzgibbon et al., 2013; Yang et al., 2020), their functions are primarily associated with secondary PD formation. Considering the critical importance of primary PD in multicellularity and the presumed lethality associated with their absence, the generation of mutants lacking primary PD remains an outstanding challenge. Additionally, due to the complex multicellularity in angiosperms compared to the simple filamentous tissue of moss protonema, observing changes in the number and density of primary PD during cytokinesis has been difficult. While the mutants of *short-leaf* (*shlf*), a unique bryophyte-specific gene that encodes tandem direct repeat-containing proteins, have a reduced PD frequency and show the change of auxin distribution pattern in gametophores (Mohanasundaram et al., 2021), the relationship between these phenotypes and the molecular functions of SHLF remains to be experimentally determined. Although SHLF was detected as a SnRK2-regulated gene in RNA-seq analysis using WT and *snrk2qKO* under ABA treatment or osmotic stress (Shinozawa et al., 2019), the relationship between SHLF and the regulatory mechanism of PD density by ABA that I found in this study is still unclear and needs further investigation.

PD density in angiosperms, although in this case primary and secondary PD are not distinguished, varies by tissue, cell type and environmental conditions (Zhu et al., 1998; Sager and Lee, 2014). However, whether a similar variation exists in bryophytes has not been previously investigated. In this

study, I have demonstrated that primary PD density indeed varies between brood cells and normal protonemal cells in *P. patens*. This observation suggests that the adjustment of cell-to-cell communication based on cell types, developmental signals, and environmental conditions may represent an essential and shared adaptive strategy among land plants. Interestingly, ABA core module and ABI5, which play crucial roles in brood cell formation, are also indispensable for the regulation of PD density by ABA (Figure 3, 4). In contrast, ABI3, which was found to be non-essential for brood cell formation, similarly does not play a crucial role in the regulation of PD density. This suggests a close coupling between ABA-induced brood cell differentiation and alterations in PD density in *P. patens*. However, overexpression of SnRK2 did not significantly change PD density, although it showed a swollen cell shape (Figure S2). This suggests that SnRK2 is essential but not sufficient for the regulation of PD density by ABA, and that other factors, such as target substrates, may also be important. In the future, it will be necessary to investigate changes in PD density in a gametophore under ABA treatment to determine whether the regulation of PD density by ABA found in this study is secondary to cell differentiation from protonemal cells to brood cells or whether it is a direct effect of ABA. Recent studies in angiosperms revealed that ABA restricts the cell-to-cell movement of viruses and the seasonal growth-promoting signal FLOWERING LOCUS T 1 via callose deposition at PD (Alazem and Lin, 2017; Tylewicz et al., 2018). However, whether ABA or its signaling components regulate primary PD density in angiosperms and whether such regulation of PD density is correlated with cell fate or the degree of cell differentiation remains to be elucidated.

In animals, connexin serves as a well-known component of gap junctions, facilitating cell-to-cell communication. Connexin exhibits a tissue-specific expression pattern (Firestone and Kapadia, 2012), and the regulation of its accumulation and degradation is crucial for gap junction formation and the modulation of their density (Segretain and Falk, 2004). In contrast, the molecular mechanisms underlying PD formation and the regulation of PD density in plants have remained elusive for over 55

years since the initial description of primary PD formation during cytokinesis (López-Sáez et al., 1966; Robards, 1976). This disparity may be attributed to the distinct structures and formation mechanisms of gap junctions and plasmodesmata, despite their shared function of molecular transport. Recent studies have revealed the localization of numerous proteins to PD (Fernandez-Calvino et al., 2011; Salmon and Bayer, 2013; Gombos et al., 2023; Johnston et al., 2023). However, whether these factors regulate PD formation, number, density, or structure remains unknown. The detailed functions of identified proteins involved in secondary PD formation are also not yet understood (Burch-Smith and Zambryski, 2010; Xu et al., 2012; Kraner et al., 2017). In conjunction with my findings, these factors offer clues to further elucidate the molecular mechanisms governing primary or secondary PD formation, density, or structure. Although factors directly involved in primary PD formation or the regulation of PD density downstream of ABA signaling have not fully been identified in the moss, studies exploring changes in gene expression and the proteome during ABA signaling have been conducted (Umezawa et al., 2013; Arif et al., 2019; Shinozawa et al., 2019). The identification of such factors will be the subject of subsequent studies.

ABA plays a pivotal role in regulating diverse terrestrial stress responses, including drought, salt, high temperature, and ultraviolet radiation, and stands as a universal phytohormone in land plants. Examination of Streptophyte algal genomes has uncovered a conserved ABA biosynthetic pathway and an incomplete yet conserved core ABA signaling module comprising SnRK2 kinases and PP2C protein phosphatases (Komatsu et al., 2020). Despite this, most algal species lack genes encoding PYR/PYL/RCAR-type ABA receptors. While some Zygnematophyceae members possess a PYR/PYL/RCAR receptor-like gene product (De Vries et al., 2018), they lack the crucial land plant–specific function of inhibiting PP2C exclusively when bound to ABA (Park et al., 2009). Instead, these proteins can interact with PP2C even in the absence of ABA (Sun et al., 2019, 2020). It is likely that the algal ancestor of all land plants acquired a mutation conferring specific activation of the

SnRK2/PP2C module by ABA. The current findings, combined with previous insights into PD permeability in *P. patens* (Tomoi et al., 2020), propose that the activation of stress resistance genes and the regulation of PD density and permeability via the ABA signaling pathway in response to abiotic stress were originally established in the common ancestor of land plants. This scenario is posited to have played a pivotal role in the successful colonization of land by plants (Figure 4E).

Figure legends

Figure 1: ABA reduces PD density in the moss *Physcomitrium patens*. (A) Brood cell differentiation upon ABA treatment. Wild-type (WT) protonemal cells before (left) and 4 d after ABA application (right). White asterisks indicate brood cells. Blue and yellow arrowheads indicate cross walls pre-formed before and newly formed after ABA application, respectively. Scale bars, 15 μm. **(B)** TEM images of WT cross walls in mock treatment and cross walls pre-formed before and newly formed after ABA application. Magenta arrowheads indicate PD on cross walls. Scale bars, 1 μm. **(C)** Quantification of PD density of WT cross walls in mock treatment and cross walls pre-formed before and newly formed after ABA application. **(D)** Chloronemal cell regeneration from brood cells. Protonema cells following treatment with ABA for 6 d (top) and 4 d, followed by 2 d of growth on ABA-free medium. Asterisk indicates a newly emerged chloronemal cell. Scale bars, 15 μm. **(E)** TEM images of cross walls formed under mock or ABA treatment (4 d) and after ABA removal (4 d). Scale bars, 1 μm. **(F)** Quantification of PD density in cross walls formed under mock or ABA treatment (4 d) and newly formed after ABA removal (4 d). **(G)** Quantification of the density of aniline blue fluorescent spots (another indication of PD density) on cross walls formed under mock treatment and cross walls pre-formed before and newly formed after ABA application. Different lowercase letters indicate significant differences among treatments ($P < 0.01$, one-way ANOVA followed by Tukey's HSD test). The bounds of the box refer to the upper (75th percentile) and lower (25th percentile) quartiles, and the whiskers refer to the lowest and highest observations. Median and mean are indicated by a bold line and a red diamond, respectively.

Figure 2: ABA reduces PD-sized pores in forming cell plates. (A) Protonemal cells of the GFP-tagged tubulin line (mock and ABA treatments). White arrows show the cell division plane. Scale bars, 15 μm. **(B)** Mature cross walls of the GFP-tubulin line (mock treatment) and newly forming cell plates

during cell division (mock and ABA treatments). Magenta arrowheads indicate PD-sized pores, and green arrows indicate pores larger than PD. Scale bars, 1 μm. **(C)** Quantification of the density of PD-sized pores or PD in GFP-tubulin in cell plates or cross walls following mock and ABA treatments as a function of cross wall thickness. **(D)** Quantification of the density of all pores of cell plates or cross walls in mock or ABA treatment. Different lowercase letters indicate significant differences among treatments ($P < 0.01$, one-way ANOVA followed by Tukey's HSD test). The bounds of the box refer to the upper (75th percentile) and lower (25th percentile) quartiles, and the whiskers refer to the lowest and highest observations. Median and mean are indicated by a bold line and a red diamond, respectively.

Figure 3: ABA core modules are essential for the ABA-induced decrease in PD density. (A) Brood cell formation after 7 d of ABA treatment in the WT, *abi3tKO*, and *snrk2qKO*. Scale bars, 15 μm. **(B)** Quantification of the density of aniline blue fluorescent spots on cross walls formed in the WT, *abi3tKO*, and *snrk2qKO* after mock or ABA treatment. **(C)** Protonemal cells in *abi1dKO* and *abi1-DN* after 4 d of 0.1% DMSO (mock) and ABA treatment. **(D)** Quantification of the density of aniline blue fluorescent spots on cross walls formed in the WT, *abi1dKO*, and *abi1-DN* after mock or ABA treatment. **(E)** Protonemal cells in *pylqKO* after 4 d of 0.1% DMSO (mock) and ABA treatment. **(F)** Quantification of the density of aniline blue fluorescent spots on cross walls formed in the WT and *pylqKO* after mock or ABA treatment. Different lowercase letters indicate significant differences between treatments ($P < 0.01$, one-way ANOVA followed by Tukey's HSD test). The bounds of the box refer to the upper (75th percentile) and lower (25th percentile) quartiles, and the whiskers refer to the lowest and highest observations. Median and mean are indicated by a bold line and a red diamond, respectively.

Figure 4: ABI5 works as a downstream factor in the regulation of PD density by ABA. (A) Protonemal cells in *abi5dKO* after 4 d of 0.1% DMSO (mock) and ABA treatment. Scale bars, 15 μm. **(B)** Quantification of the density of aniline blue fluorescent spots on cross walls formed in *abi5dKO* after mock or ABA treatment. **(C)** WT protonemal cells after 7 d of 0.1% DMSO (mock), 0.1 M mannitol, or 0.3 M mannitol treatment. Scale bars, 15 μm. **(D)** Quantification of the density of aniline blue fluorescent spots on WT cross walls following 7 d of mock, 0.1 M mannitol, or 0.3 M mannitol treatment. Different lowercase letters indicate significant differences between treatments ($P < 0.01$, one-way ANOVA followed by Tukey's HSD test). The bounds of the box refer to the upper (75th percentile) and lower (25th percentile) quartiles, and the whiskers refer to the lowest and highest observations. Median and mean are indicated by a bold line and a red diamond, respectively. **(E)** A model of the role of the ABA core signaling module in stress resistance, cell fate decision, and cell-to-cell communication by regulating PD density and permeability. The pathways found in this study are shown in red.

Supplementary Figure S1: ABA affects PD number and its density. (A) Quantification of PD number on the sections of cross walls in the mock or ABA-treated WT using TEM ($P < 0.01$, Welch's t-test). Note that the overall length of cross walls varies depending on the sectioning location. **(B)** PD structure in cross walls (mock and ABA treatments). Scale bars, 200 nm. **(C)** Quantification of the width of PD aperture in cross walls under mock treatment or cross walls pre-formed before and newly formed after ABA application. **(D)** Sequence of steps for SRRF image analysis of a WT cross wall. Top to bottom: bright-field image (BF), aniline blue fluorescence image, image obtained with the ImageJ plug-in SRRF. Scale bars, 4 μm. **(E)** Quantification of the density of aniline blue fluorescent spots in cross walls formed under ABA treatment with different concentrations. Different lowercase letters indicate significant differences between treatments ($P < 0.01$, one-way ANOVA followed by

Tukey's HSD test). The bounds of the box refer to the upper (75th percentile) and lower (25th percentile) quartiles, and the whiskers refer to the lowest and highest observations. Median and mean are indicated by a line and a red diamond, respectively.

Supplementary Figure S2: Overexpressing ABI3 and SnRK2 does not affect PD density. (A) Protonemal cells of WT, *abi3 tKO*, and *snrk2 qKO* before ABA application. Scale bars, 10 µm. **(B)** Protonemal cells of *ABI3A*-inducible overexpression line (*ABI3iox*) under mock and β-estradiol treatment. **(C)** Quantification of the density of aniline blue fluorescent spots in the *ABI3iox* cross walls formed under mock treatment or pre-formed before and newly formed after the induction of overexpression by β-estradiol. **(D)** Protonemal cells of *Snrk2A*-inducible overexpression line (*SnRK2iox*) under mock and β-estradiol treatment. **(E)** Quantification of the density of aniline blue fluorescent spots in the *SnRK2iox* cross walls formed under mock treatment or pre-formed before and newly formed after β-estradiol or ABA application. Different lowercase letters indicate significant differences between treatments ($P < 0.01$, one-way ANOVA followed by Tukey's HSD test). The bounds of the box refer to the upper (75th percentile) and lower (25th percentile) quartiles, and the whiskers refer to the lowest and highest observations. Median and mean are indicated by a line and a red diamond, respectively.

Supplementary Figure S3: Phylogenetic tree of PYL receptors. A non-rooted maximum-likelihood phylogenetic tree was constructed using the LG as substitution model. Letters of branches denote bootstrap support based on 100 repetitions. The bar represents the number of amino acid changes per branch length.

Supplementary Figure S4: *snrk2qKO* show higher sensitivity for mannitol treatment. Protonemal

cells in WT (left) and *snrk2qKO* (right) cultured under 0.3 M mannitol treatment. Scale bars, 30 μm.

Chapter 3; Contribution of GGB-ROP signaling to PD formation and its relationship with ABA signaling in the moss *Physcomitrium patens*

Abstract

In land plants, Rho of plants (ROP), a small GTPase, plays a crucial role in regulating cell polarity. In the moss *P. patens*, a complete deficiency of ROP results in a distinctive phenotype marked by a lack of multicellularity that resembles brood cells which is stress-tolerant cells induced by abscisic acid (ABA). Given that ABA signal functions partly antagonistically with ROP signal, I hypothesized that ROP mutants exhibit a reduction in plasmodesmata (PD) density. My observations indeed confirmed a decrease in PD density in ROP mutants. I next investigated factors associated with ROP and Formin as a candidate downstream component, and found a reduction in PD density in these mutants. This highlights the importance of these proteins in PD formation.

Introduction

As described in Chapter 1, the evolutionary progression towards multicellularity involves the acquisition of essential traits such as cell adhesion, cell polarity, cell-to-cell communication, cell differentiation, and various regulatory mechanisms. These traits are tightly linked rather than independently regulated, forming a complex network of interactions crucial for sustaining the multicellular state. For instance, the establishment of cellular polarity during division can lead to asymmetric cell division, resulting in daughter cells with distinct characteristics that eventually drive cell differentiation. For example, it is documented that novel cell-to-cell communication can emerge at the site of cell-cell attachment, exemplified by grafting in plants (Kurotani and Notaguchi, 2021). Nevertheless, the details of individual regulation within these traits and their collective contribution to the maintenance of the multicellular state remain unresolved. In this Chapter 3, my analysis has centered on factors related to cell polarity. Thus, I have identified a set of factors that commonly play a role in the regulation of cell polarity and are implicated in PD formation.

The Rho family of small GTPase proteins (Rho, Rac, Cdc42 and ROP/RAC) are known to play important roles in various processes that create cell polarity (Jaffe and Hall, 2005; Feiguelman et al., 2018). ROP (Rho of plants), also called RAC, resides in a plant-specific clade of Rho-GTPases and is implicated in the morphogenesis of leaf epidermal cells (Craddock et al., 2012), polarized growth of root hairs and pollen tubes, with its activation or deactivation modulated by auxin and ABA signaling, respectively (Feiguelman et al., 2018). However, the regulatory mechanisms underlying these processes remain largely elusive. Similar to other Rho family GTPases, ROP functions as a signaling switch, oscillating between the GTP-bound active state and the GDP-bound inactive state. This cycling is intricately regulated by various factors, including GEF, GAP, and GDI. In *Arabidopsis thaliana*, the ROP family consists of 11 members with high sequence identity, categorizable into 4 subgroups (Zheng and Yang, 2000). Several studies have proposed the involvement of certain ROP family

members in the ABA signaling pathway. For instance, the expression of a constitutively active form of ROP6 led to a reduction in ABA-mediated stomatal closure (Lemichez et al., 2001). Zheng et al. (Zheng et al., 2002) demonstrated that ROP10 serves as a specific negative regulator of multiple ABA responses, including ABA-mediated stomatal closure, seed germination, and root elongation, using knockout lines. Additionally, ROP11 has been identified as a negative regulator of various ABA responses (Li et al., 2012) .

The protonema of *P. patens* has a simple multicellular body. It consists of exposed cells connecting linearly, with apical cells constantly growing apically (tip growth) and maintaining proliferative activity. In *P. patens*, ROP family comprises four members, all sharing high sequence identity. ROP has been consistently observed to exhibit strong localization at the tip region of apical cells (Cheng et al., 2020; Yi and Goshima, 2020). The complete deficiency of ROP fails to generate a three-dimensional multicellular structure, known as the gametophore, and displays a rounded cell shape, reminiscent of ABA-induced brood cells (Cheng et al., 2020).

In Chapter 1, I investigated the cellular physiological changes induced by ABA on the cell polarity of protonemal apical cells. In Chapter 2, my findings indicated the involvement of ABA in the regulation of PD density, crucial for cell-to-cell communication. Utilizing confocal microscopy with aniline blue staining and transmission electron microscopy (TEM), I demonstrated the significance of the ROP signal in PD formation. Additionally, as a candidate factor which works in the same pathway with ROP, Formin, a recognized effector of the Rho protein in animals (Kühn and Geyer, 2014) and furthermore, actin may function on PD formation.

Material and methods

Plant materials and growth conditions

The moss *Physcomitrium patens* (Hedw., formerly *Physcomitrella patens*) Bruch & Schimp accession Gransden was used in this study as the wild type. *rop1/3/4tKO*, *rop 1/2/3/4qKO* and Rop-swmNG are described previously (Cheng et al., 2020). *ggbko* and *pGX8-ROP-amiRNA* are described previously (Thole et al., 2014; Bao et al., 2022). Transient RNAi assays for ROP regulators or Formin were performed in a line stably expressing NLS-GFP-GUS (Bezanilla et al., 2005). All plants were subcultured on BCDAT medium solidified with 0.8% (w/v) agar (Nacalai Tesque) under continuous white light (30 μmol m^{-2} s^{-1}) at 25 °C (Nishiyama, 2000).

Establishment of the *pGX8-PpRop2* line

The ORF fragment of *PpRop2* was amplified with the primer set of 5'-CACCCGCAGAGAGTTGGGAGGAGTG-3' (forward) and 5 '-CACCTGGGTGACTCGGTTCGTGTT-3' (reverse). The resultant plasmid was subjected to LR reaction with the destination *pPGX8* (Kubo et al., 2013) using the LR clonase II plus enzyme mix. The plasmids *pGX8-PpRop2* were digested with the restriction enzyme *Sse*8387I (Takara Bio) for gene targeting and introduced into wild-type *P. patens* by polyethylene glycol-mediated transformation, as described previously (Nishiyama, 2000). Stable transformants were selected twice on BCDAT agar medium containing 30 mg/l hygromycin B (Wako).

Transient RNAi assays

Protoplasts were transformed by polyethylene glycol-mediated transformation, as described

previously (Nishiyama et al., 2000). RNAi plasmids for ROP regulators and Formin are described previously (Vidali et al., 2009; Bascom et al., 2019). The RNAi plasmids contained a hygromycin-resistance cassette, and therefore regenerating plants were transferred to standard growth media supplemented with 15 μg / ml hygromycin 4 d after transformation. Plants were imaged 7 d after transformation using an inverted microscope (ECLIPSE Ti-E, Nikon) with a FITC filter. Living plants were visually screened for active silencing of the NLS-GFP-GUS marker.

Treatment and observation of protonemata

Protonemata tissues were prepared in glass-bottom dishes (or four-well glass-bottom chamber; Iwaki) to enable detailed observations of the cross wall position under an inverted microscope (ECLIPSE Ti-E, Nikon) or an upright microscope (BX60, Orympus). BCDATG (BCDAT and 0.5% [w/v] glucose) solidified with 0.8% agar (w/v) was used as culture medium. After the moss was transplanted to the bottom of the chamber, the chamber was turned upside down and incubated under continuous red light (20 μmol m^{-2} s^{-1}) for 5-7 d. The position of the septa was checked under before and 4 d after the application of 0.1% (v/v) DMSO (mock treatment) or 1 μM β-est.

Transmission electron microscopy

Protonemata tissues were fixed in 3% (w/v) glutaraldehyde (Nisshin EM) and 1% (w/v) formaldehyde (freshly prepared from paraformaldehyde, TAAB) in 0. After rinsing in 0.1 M sodium phosphate buffer, the material was post-fixed with 1% (w/v) osmium tetroxide (Nisshin EM) in 0.1 M sodium phosphate buffer, pH 6.8, overnight at 4°C, dehydrated through an ethanol series, and embedded in Spurr resin (mixing ERL4221, DER736, NSA [Polysciences]). Sections were sequentially stained with EM Stainer (Nisshin EM) for 30 min, stained with lead stain solution (Sigma-Aldrich Japan) for 8 min,

and examined Sections were sequentially stained with EM Stainer (Nisshin EM) for 30 min, stained with lead stain solution (Sigma-Aldrich) for 8 min, and examined under a H-7650 transmission electron microscope (Hitachi High-Tech).

Aniline blue staining

Aniline blue (Biosupplies) was dissolved in sterile water to 1 mg/ml and stored as a stock solution at 4°C in the dark. When glass-bottom chambers were used, fresh solutions were prepared by diluting the solution to 330 μg/ml in 100 mM phosphate buffer (pH 8.5) and used to treat samples for 1 d before observation at a final concentration of 33 μg/ml. Moss plantlets grown in liquid medium were picked out and placed in fresh solution diluted to 33 μg/ml in 100 mM phosphate buffer (pH 8.5) and incubated at room temperature for 30 min. Aniline blue fluorescence was detected under a Zeiss LSM980 confocal microscope equipped with a Plan-Apochromat 63×/1.40 oil DIC M27 objective. A 405-nm laser with 0.2% power intensity was used to excite aniline blue. The detection range was 410–605 nm. Fluorescence spot density was measured based on super resolution radial fluctuation (SRRF) images. NanoJ-SRRF (Gustafsson et al., 2016), a plug-in for ImageJ (Fiji), was used to obtain one SRRF image from 10 consecutive images. The number of spots was counted in ImageJ, and spot density was calculated based on the length of the area where aniline blue fluorescence was observed in the cross walls.

Analysis of ROP localization and quantification

ROP-mNeonGreen fluorescence was detected under a Zeiss LSM980 confocal microscope equipped with a Plan-Apochromat 63×/1.40 oil DIC M27 objective. Laser illumination at 488 nm was used for mNeonGreen excitation. Emission filters were 525/50 nm. Time-lapse and Z-stack image acquisition

was controlled by ZEISS ZEN (blue edition). ROP clusters were extracted from fluorescent images using ImageJ with filters and Auto Threshold, and counted using Analyze Particles.

Quantification and statistical analysis

The density of aniline blue fluorescent spots on cross walls was quantified using Fiji-ImageJ. Statistical analyses were performed using R ver. 4.0.2. For the multiple sample comparison, one-way ANOVA with post-hoc Tukey HSD test was performed (Tukey, 1949). Graphs were generated using the R ggplot2 package, BoxPlotR, or Microsoft Excel. The value of n indicates the number of samples. Statistical significance is defined in the figure legends.

Results

Loss of ROP results in a significant reduction in PD density

I focused on the cell morphology of *ROP* knockout mutants, as described by (Cheng et al., 2020), which is similar to brood cells in Chapter I and II showing the loss of multicellularity. Subsequently, cross walls in the mutants were examined to investigate potential significant changes in PD, a vital component for cell-to-cell communication. In comparison to the cylindrical protonema of the wild type (WT), both *rop134* triple knockout (*roptKO*) and *rop1234* quadruple knockout (*ropqKO*) mutants exhibited shorter or rounded individual cells (Figure 1A). In *A. thaliana*, Type 1 ROP with a CaaL motif at the C-terminus have been reported to undergo prenylation by protein geranylgeranyl transferase (PGGT) and anchor to the plasma membrane (Sorek et al., 2011). In *P. patens*, a *ggb* knockout (*ggbKO*) mutant lacking the β-subunit of PGGT also displayed a round cell morphology similar to that of *rop1234qKO* (Thole et al., 2014) (Figure 1A). Observation of cross walls in these mutants by transmission electron microscopy (TEM) showed that the number of PD was greatly reduced in all of them (Figure 1B). Quantitative analysis of PD density on cross walls in these mutants among TEM observation demonstrated its reduction compared to WT (Figure 1C). With aniline blue staining, which stains callose preferentially accumulating at PD (Method is the same as Chapter 2), a decrease in fluorescent spot density was observed compared to WT (Figure 1D). These findings suggest the involvement of ROP and PGGT in PD formation. It has been reported that callose is more uniformly distributed in *ggbKO* than in WT, where callose is restricted to cross walls, according to the observation using callose antibodies (Thole et al., 2014). Therefore, the reason for the weaker decrease in PD density using aniline blue staining (Figure 1D) compared to TEM observation (Figure 1C) suggests the possibility that callose accumulation also occurred outside of the PD and was detected.

Additionally, it has been reported that in *P. patens*, protonemal cells exhibit a rounded cell morphology when ROP is overexpressed or knocked down, similar to *rop123tKO* and *rop1234qKO*

mutants (Ito et al., 2014; Burkart et al., 2015). Thus, in this study, a β-estradiol (β-est) inducible *ROP-amiRNA* line (Bao et al., 2015), which suppressed ROP expression by artificial micro RNA was used to investigate the impact of ROP levels on PD density. Upon induction of *ROP* knockdown, chloroplasts increased in density, resembling the effect of ABA treatment and *rop* knockout mutants, and cells exhibited shortened and rounded lengths (Figure 2A). In this analysis, I distinguished cross walls formed before and after induction of *ROP* knockdown and observed PD in the cross walls (old v.s. new in Figure 2B). PD density was significantly reduced in cross walls formed after *ROP* knockdown (Figure 2C); the same trend also confirmed by aniline blue staining (Figure 2D). In addition, after removal of β-est and culture β-est-free medium, PD were observed at the same level as mock in newly formed cross walls and PD density was restored (Figure 2B). This suggests that a reduction in ROP abundance influences PD formation. To further investigate the relationship between ROP levels and PD density, I generated β-est inducible ROP overexpression lines (Figure S1A), *pGX8-Rop2* and found that *ROP* overexpression led to a decrease in PD density (Figure S1B, C), similar to the effect observed with *ROP* knockdown. In *Arabidopsis* pollen tubes, both *ROP* overexpression and functional inhibition by antibodies disrupt apical actin organization (Lin and Yang, 1997; Kost et al., 2000). Given these reports, the reduction in PD density in ROP knockdown and overexpression lines suggests that the amount of ROP present is strictly regulated in PD formation, but another possibility is that ROP cycling between active and inactive forms is crucial in PD formation.

Regulators of ROP are crucial in PD formation, and Class II Formin and actin may participate in same pathway

Since ROP has been suggested to be an important factor in PD formation, I explored the potential involvement of ROP regulators, such as ROPGAP, ROPGEF, and ROPGDI, in this regulatory process. Using transient RNAi expressors for each ROP regulators (Bascom et al., 2019), I observed disrupted

cell polarity, which is reminiscent of *rop1234qKO* in the cell morphology of each of the mutants (Figure 3A). TEM analysis of the mutants' cross walls confirmed the reduction in the number and density of PD (Figure 3B, C). In addition, since Formin is widely recognized as one of the effectors of Rho proteins in animals (Kühn and Geyer, 2014), I chose Formin as a candidate factor which works in the same pathway with ROP. Both proteins exhibit co-localization in the apical tip of the protonema in *P. patens* (Cheng et al., 2020; Van Gisbergen et al., 2020), although direct interaction between ROP and Formin has not been confirmed to date, implying their cooperative involvement in actin dynamics (Burkart et al., 2015; Van Gisbergen et al., 2020). In *P. patens*, three Formin groups exist: Class I, Class II, and Class III, with Class III found in mosses and ferns and not in angiosperms (Grunt et al., 2008). In Class I and Class II RNAi plants, the former exhibits a cylindrical cell shape, while the latter displays a rounded cell morphology with attenuated cell polarity (Figure 3A). This cell morphology of Class II RNAi plants is similar to RNAi plants of ROP or its regulators (Vidali et al., 2009). By observing each cross wall by TEM (Figure 3B) and measuring their PD density, I revealed that RNAi of Class II Formin significantly reduced PD density, but not the one of Class I Formin (Figure 3C). These results suggest that Class II Formin may function the same or overlapping processes of ROP in PD formation. Additionally, I used Latrunculin B (LatB), an inhibitor of actin polymerization, to determine whether PD density is altered when actin dynamics are disrupted, since both ROP and Formin are involved in regulating actin dynamics. LatB-treated protonema exhibited a short and round cell morphology (Figure 3D). Quantification of aniline blue fluorescent spots demonstrated that LatB treatment reduced its fluorescent spot density (Figure 3E). Taken together, these results suggest that ROP is involved in PD formation, highlighting the importance of regulating ROP activation and inactivation, and actin downstream of ROP along with Formin regarding PD formation.

ROP forms nanodomain structures on the plasma membrane, and ABA affects the size and

density of these nanodomain structures

My previous data have indicated that ABA can suppress PD formation (Chapter 2) and that ROP plays a role in PD formation. Therefore, I investigated how the localization of ROP is altered by ABA using ROP-swmNeonGreen (Cheng et al., 2020). I observed ROP localization at the apical tip of the protonema but was also present at the cell cortex and at the cell division plane during cell division (Figure 4A, B). I noticed the punctate signals as ROP nanodomain in the cell cortex. Following ABA treatment, the fluorescence signal in the tip region gradually decreased within 2 hours (Figure 4C), and the nanodomain structure near the cell cortex weakened at 2 hours after ABA treatment (Figure 4D), where its size was reduced (Figure 4E). Additionally, 2 days after ABA treatment, granule-like structures larger than the nanodomain were observed neat the cell cortex (Figure 4F). This implies that ABA influences the distribution and size of ROP nanodomain and the cycling of ROP on the plasma membrane.

Discussion

GGB-ROP signaling is crucial for PD formation

This study reveals the significance of prenylated and plasma membrane-anchored ROP in PD formation because ROP knockout or ROP regulators RNAi lead to a substantial reduction in PD density. Given that moss plants lack the ability to form secondary PD (Evkaikina et al., 2014), this signaling pathway likely plays a crucial role in controlling primary PD formation. PD are essential for multicellularity of land plants, and their complete absence is assumed to be lethal; hence, mutants completely lacking primary PD have not been successfully obtained (Brunkard and Zambryski, 2017). However, I found that the density of primary PD decreases in an ABA-dependent manner under stress, as described in Chapter 2. Moreover, *short-leaf* in *P. patens* with reduced PD density has been recently reported in (Mohanasundaram et al., 2021). This gene is a moss-specific gene, which encodes a protein with a tandem direct repeat (TDR), and its mutation has been reported to affect auxin distribution in the gametophore, but the function of this gene product and the molecular mechanisms involved in PD density are still unknown. Thus, I reveal the importance of the ROP and its related proteins in PD formation by analyzing multiple gene mutants that exhibit reduced PD density.

ABA alters ROP localization and domain distribution

This study reveals that ABA induces alterations in the domain distribution and size of ROP within the surface layer of moss protonemal apical cells (Figure 4). Previous research in *Arabidopsis* roots suggested that ROP6 forms nanodomains in response to osmotic signal and recruit effectors for ROS production as a second messenger (Smokvarska et al., 2020). Moreover, in secondary cell wall patterning, active ROP11 has been shown to create domain patterns inducing secondary wall pores formation by depolymerizing surface microtubules (Oda and Fukuda, 2012). Also, a recent study have proposed that activator ROPGEF and inhibitor ROPGAP generate various two-dimensional patterns

through a reaction-diffusion system (Smokvarska et al., 2021) While the nanodomain structure of ROP has been recently observed in the moss, *P. patens* (Ruan et al., 2023), nanodomain on cell plate has not been reported and its function or changes under environmental stimuli or developmental stage remain to be determined experimentally. While reports in *Arabidopsis* epidermal cells suggest that ABA promotes ROPGEF degradation (Li et al., 2016), further investigation is required to ascertain the conservation of this regulatory pathway of ROPGEF by ABA in *P. patens*. Additionally, it is crucial to determine whether changes in the nanodomain structure of ROP are implicated to recruit some effectors in the response of environmental stimuli including osmotic stress and cell morphological changes in *P. patens*, as observed in *Arabidopsis*. Furthermore, exploring the relationship between the ROP nanodomain and PD density is essential for a comprehensive understanding of these processes.

ROP may regulate actin dynamics in phragmoplasts together with Formin

I investigated Formin as a potential factor working with ROP, and showed that RNAi targeting Class II Formin results in a reduction of PD density. Formin, recognized for its interaction with actin filaments, facilitates actin nucleation and polymerization (Deeks et al., 2002). An assessment of PD density changes using the actin polymerization inhibitor Latrunculin B demonstrated a decrease of PD density in the cross walls, suggesting the involvement of the actin cytoskeleton downstream of ROP signaling in PD formation. In cell division of land plants, the phragmoplast consists of actin filaments and microtubules, with vesicular transporters, membrane compartments, and regulatory proteins being present together. PD formation occurs at the cell plate, expanding through vesicular transport involving the plasma membrane and cell wall components. Both ROP and Formin in *P. patens* have been documented to localize at the cell division plane (van Gisbergen et al., 2012; Cheng et al., 2020). Moreover, Formin has been observed to create domain structures at the cell surface like ROP (van Gisbergen et al., 2012; Van Gisbergen et al., 2020). Integrating these insights with the observed domain

structures of ROP at the cell surface, a hypothesis emerges that ROP and Formin, typically concentrated on the apical side of apical cells, orchestrate vesicular transport through the cytoskeleton (Figure S2A, 2B), and at the same time, they may form a nanodomain in the cell division plane, regulating the cytoskeleton, especially in phragmoplasts, to transport cell wall-related enzymes to the cell plate. This process could facilitate the maintenance of pores, resulting in the establishment of PD (Figure S2C). Further investigation of the domain structure of ROP and Formin in the cell division plane, along with the identification of cell wall-related enzymes recruited to vesicular transporters, will be crucial in uncovering the key factors involved in PD formation.

Figures legends

Figure 1: Loss of ROP greatly reduces PD density. (A) Protonemal cells in WT, *rop134tKO*, *ropqKO* and *ggbKO*. Scale bars, 20 μm. **(B)** Cross walls of WT, *rop134tKO*, *ropqKO* and *ggbKO*. Magenta arrowheads indicate PD. Scale bars, 1 μm. **(C)** Quantification of the density of PD in WT, *rop134tKO*, *ropqKO* and *ggbKO* ($P < 0.01$, Welch's t-test). **(D)** Quantification of the density of aniline blue fluorescent spots in cross walls in WT, *rop134tKO*, *ropqKO* and *ggbKO.* Different lowercase letters indicate significant differences between treatments ($P < 0.01$, one-way ANOVA followed by Tukey's HSD test). The bounds of the box refer to the upper (75th percentile) and lower (25th percentile) quartiles, and the whiskers refer to the lowest and highest observations. Median and mean are indicated by a bold line and a cross, respectively.

Figure 2: *Rop* knockdown mimic the phenotype of *rop134 tKO*. (A) Protonemal cells of *pGX8-Rop ami RNA* line under mock and 4 days of β-est (inducing overexpression of artificial micro RNA of *Rop*) treatment. Scale bars, 20 μm. **(B)** TEM images of *pGX8-Rop ami RNA* cross walls in mock-treated protonema and in protonemata before and after β-est treatment. Most below image is a cross wall which newly formed in re-culturing after β-est removal. Magenta arrowheads indicate PD on cross walls. Scale bars, 1 μm. **(C)** Quantification of the density of PD in *pGX8-Rop ami RNA* cross walls in mock-treated protonema and in protonemata before and after β-est treatment or β-est removal. **(D)** Quantification of the density of aniline blue fluorescent spots in cross walls in *pGX8-Rop ami RNA* cross walls in mock-treated protonema and in protonemata before and after β-est treatment. Different lowercase letters indicate significant differences between treatments ($P < 0.01$, one-way ANOVA followed by Tukey's HSD test). The bounds of the box refer to the upper (75th percentile) and lower (25th percentile) quartiles, and the whiskers refer to the lowest and highest observations. Median and mean are indicated by a bold line and a cross, respectively.

Figure 3: RNAi of ROP regulators or class II Formin decreased PD density. (A) Protonemal cells of NLS-GFP-GUS line transformed with a construct silencing the indicated gene family. Scale bars, 20 μm. **(B)** TEM images of cross walls in each RNAi plants transformed with a construct silencing the indicated gene family. Magenta arrowheads indicate PD on cross walls. Scale bars, 1 μm. **(C)** Quantification of the density of PD in each RNAi plants cross walls transformed with a construct silencing the indicated gene family. (n = 17, 23, 43, 17, 28, 39 cross walls, respectively.) **(D)** Protonemal cells of WT under 4 days of mock or 0.5 μM LatB treatment. Scale bars, 20 μm. **(E)** Quantification of the density of aniline blue fluorescent spots in cross walls under 4 days of mock or LatB treatment. Different lowercase letters indicate significant differences between treatments ($P <$ 0.01, one-way ANOVA followed by Tukey's HSD test). The bounds of the box refer to the upper (75th percentile) and lower (25th percentile) quartiles, and the whiskers refer to the lowest and highest observations. Median and mean are indicated by a bold line and a cross, respectively.

Figure 4: ABA affects ROP nanodomain pattern. (A) ROP-mNeonGreen localization in an apical cell (top) and a cell division plane (Bottom). 5–8 independent apical cells and 3 independent cell division planes were observed with a confocal microscope. Scale bars, 10 μm. **(B)** Single plane of different z-stack of ROP-mNeonGreen. Interval scale of z-stack is 0.4 μm. Scale bars, 5 μm. **(C)** Max projection of ROP-mNeonGreen at the tip region in ABA treatment. 5 independent apical cells were observed with a confocal microscope. Scale bars, 5 μm. **(D)** Single plane of cell cortex of ROP-mNeonGreen in ABA treatment. White arrowheads indicate some samples of the nanodomain. 3 independent apical cells were observed with a confocal microscope. **(E)** Quantification of ROP cluster size. Single plane of cell cortex of ROP-mNeonGreen in ABA treatment. All nanodomains larger than or equal 0.01 μm² of 3 independent apical cells in 0 hour or 2 hours ABA treatment were counted and

the size distribution was shown in a violin plot ($P < 0.01$, Wilcoxon rank sum test). Mean is indicated by a red point. **(F)** Aggregation of ROP-mNeonGreen in 2 days ABA treatment. White arrowheads indicate some samples of aggregation.

Figure S1: *Rop* overexpression decrease PD density. (A) Protonemal cells of *pGX8-Rop2* under mock and 4 days of β-est (inducing *Rop* knock dowm) treatment. Scale bars, 20 μm. **(B)** TEM images of *pGX8-Rop2* cross walls in mock-treated or β-est treated protonema. Magenta arrowheads indicate PD on cross walls. Scale bars, 1 μm. **(C)** Quantification of the density of PD in *pGX8-Rop2* cross walls in mock-treated or β-est treated protonema. Different lowercase letters indicate significant differences between treatments ($P < 0.01$, one-way ANOVA followed by Tukey's HSD test). The bounds of the box refer to the upper (75th percentile) and lower (25th percentile) quartiles, and the whiskers refer to the lowest and highest observations. Median and mean are indicated by a bold line and a cross, respectively.

Figure S2: Proposed model of the function of ROP and Formin in the PD formation. (A) Tip growth and cell division plane in *P. patens* protonemal cells. ROP and Formin localize at tip region and cell division plane and organize cytoskeleton. Actin filaments (red lines) and microtubules (green lines) have interacted each other. Tip region and cell division plane (dashed frame) are enlarged in **(B)** and **(C)**, respectively.

Figure S3: Phylogeny of the Streptophyta with focus on the occurrence of phragmoplast and PD or PD like structures. The phylogeny and existence of phragmoplast and PD or PD like structures based on the reviews (Buschmann and Zachgo, 2016; Brunkard and Zambryski, 2017; Wegner et al., 2023). Only groups that have been examined for the presence of phragmoplast or PD / PD-like

structure are shown.

General discussion

This study elucidates the impact of ABA on the intricate cell polarity of the cytoskeleton during brood cell formation, as well as its role in diminishing the mitotic activity of the stress-resistant stem cells (Chapter 1). The unaltered mitotic activity in *snrk2qKO* in ABA treatment suggests the indispensability of the ABA core module including SnRK2 in this regulatory process. Additionally, *abi3tKO* induces brood cells by ABA, whereas *abi5dKO* shows an absence of brood cells, indicating that ABI5 but not ABI3 plays an important role downstream of the ABA core module in the regulation of brood cell formation. It has been reported that cell-to-cell communication is suppressed in brood cells (Kitagawa and Fujita, 2015), and in addition, regulation of PD permeability via SnRK2 and partially ABI3 has been reported as a PD regulation independent of callose by ABA (Tomoi et al., 2020). Here I further found a pivotal function of ABA on PD formation as in Chapter 2 that the ABA core module is essential for the control of PD density, and that ABI5 functions downstream of it. In other words, ABI3 and ABI5 different transcription factors may be used to regulate PD permeability and density differently in their regulation.

ABA is synthesized under stress conditions and triggers various stress responses. My observations suggest that ABA impedes PD formation. Consequently, under abiotic stress conditions, ABA suppresses PD density by inhibiting the regulatory system responsible for PD formation with the regulation of PD permeability, which leads to the suppression of cell-to-cell communication. What, then, are the PD formation mechanisms that ABA suppresses? I focused mutants of ROP and ROP-related genes exhibiting a phenotype where cells are detached from each other. This is similar to the brood cells, where as a diaspore, brood cells are also easily detached from each other. In these ROP and ROP-related mutants, I found a reduction in PD density. Considering the antagonistic relationship between ROP and ABA signaling, I propose that the ABA-induced decline in PD density results from alterations in ROP signaling. Indeed, my investigations revealed that ABA supplementation led to

changes in ROP localization and nanodomain structure. Based on these findings, I hypothesize that the PD formation mechanism by ROP may be suppressed by stress or ABA.

Proper regulation of cell polarity and cell-to-cell communication is crucial in multicellular organisms. This study suggests that ROP signaling factors contributing to cell tip growth, specifically polarized growth, also play a role in PD formation during cell division. I propose that ROP and Formin, responsible for organizing the cytoskeleton and recruiting vesicular transporters at the tip of apical cells, similarly regulate the cytoskeleton at the cell plate. They may function to facilitate the transport of a downstream factor of PD formation like a cell wall enzyme, to these sites, initiating PD formation through vesicular transport (Figure S2). Future research is expected to involve a more detailed observation and simulation of the domain pattern of ROP, as well as the identification of execution factor for forming and maintaining the PD pores in the cell plate.

Although the PD-like structure of cytoplasmic connecting structures in Coleochaetophyceae and Charophyceae differs somewhat from PD of land plants, they are absent in Zygnematophyceae, considered the sister group of land plants (Wegner et al., 2023)(Figure S3). Land plants PD are composed inner membrane continuous with the plasma membrane, desmotubule continuous with ER. In contrast, in Coleochaetophyceae, PD-like structures have been reported in only several species of genus *Coleochaete*, and no reports of visible internal structures in their PD. In Charophyceae, only *Chara* and *Nitella* have been reported to have PD like structure, and there are varying reports on the presence/absence of an internal PD-like structure, which might be associated/not associated with the ER, and is occasionally attached to the plasma membrane via spoke-like connections. All groups exhibiting this PD-like structure have been found to form phragmoplasts during mitosis (Buschmann and Zachgo, 2016). Consequently, it has been suggested that the phragmoplast was a necessary precursor for the evolutionary origin of the PD-like structure in the Charophyceae and Coleochaetophyceae lineage (Graham et al., 2000), however, the debate continues regarding whether

the origin of PD and PD-like structures in Phragmoplastophyta is the same (Wegner et al., 2023). Brown and red algae also exhibit cytoplasmic connecting structures, which are believed to have a distinct origin from land plant PD. However, much remains unknown about how these structures form, including the molecular mechanisms involved. If there is a shared mechanism, as hypothesized here for PD formation involving ROP and Formin, wherein the cytoskeleton is regulated to create and maintain pores by transporting specific substances to precise locations through vesicular transport, this would represent a crucial mechanism in acquiring cell-to-cell communication. Nevertheless, due to the diversity of cell wall components, it is expected that there should be also a wide variety of PD pore-forming execution factors.

Acknowledgments

I would like to sincerely thank my supervisor Dr. Tomomichi Fujita for his mentorship, guidance, and support during my Ph.D. He patiently guided me from the beginning of my studies to the writing of my doctoral dissertation.

I would like to deeply thank Dr. Chikako Nagasato, Dr. Ryohei Thomas Nakano, and Dr. Satoshi Naramoto for kindly accepting a sub-chief examiner of my doctoral dissertation and constructive suggestions and comments.

I also thank Dr. Daisuke Takezawa and Dr. Yoichi Sakata for providing *pylqKO* and *abi5dKO*. I also thank Dr. Bezanilla Magdalena for providing *rop134tKO*, *rop1234qKO*, ROP-swmNeonGreen and RNAi constructs of ROP regulators or Formin.

I thank my family and all the members in Keitai 1 Laboratory for their support and helpful discussion.

This work was supported by a Sasakawa Scientific Research Grant from The Japan Science Society and Hokkaido University Ambitious Doctoral Fellowship (Information Science/AI).

References

Alazem, M., and Lin, N. S. (2017). Antiviral roles of abscisic acid in plants. *Front Plant Sci* 8. doi: 10.3389/fpls.2017.01760

Arif, M. A., Hiss, M., Tomek, M., Busch, H., Meyberg, R., Tintelnot, S., et al. (2019). ABA-induced vegetative diaspore formation in *Physcomitrella patens*. *Front Plant Sci* 10. doi: 10.3389/fpls.2019.00315

Bao, L., Ren, J., Nguyen, M., Slusarczyk, A. S., Thole, J. M., Martinez, S. P., et al. (2022). The cellular function of ROP GTPase prenylation is important for multicellularity in the moss *Physcomitrium patens*. *Development (Cambridge)* 149. doi: 10.1242/dev.200279

Bao, L., Yamamoto, K. T., and Fujita, T. (2015). Phototropism in gametophytic shoots of the moss *Physcomitrella patens*. *Plant Signal Behav* 10. doi: 10.1080/15592324.2015.1010900

Bascom, C., Burkart, G. M., Mallett, D. R., O'Sullivan, J. E., Tomaszewski, A. J., Walsh, K., et al. (2019). Systematic survey of the function of ROP regulators and effectors during tip growth in the moss *Physcomitrella patens*. *J Exp Bot* 70. doi: 10.1093/jxb/ery376

Bezanilla, M., Perroud, P. F., Pan, A., Klueh, P., and Quatrano, R. S. (2005). An RNAi system in *Physcomitrella patens* with an internal marker for silencing allows for rapid identification of loss of function phenotypes. *Plant Biol* 7. doi: 10.1055/s-2005-837597

Bloemendal, S., and Kück, U. (2013). Cell-to-cell communication in plants, animals, and fungi: A comparative review. *Naturwissenschaften* 100. doi: 10.1007/s00114-012-0988-z

Bowman, J. L. (2022). The origin of a land flora. *Nat Plants* 8, 1352–1369. doi: 10.1038/s41477-022-01283-y

Brunkard, J. O., and Zambryski, P. C. (2017). Plasmodesmata enable multicellularity: new insights into their evolution, biogenesis, and functions in development and immunity. *Curr Opin Plant Biol* 35. doi: 10.1016/j.pbi.2016.11.007

Burch-Smith, T. M., Stonebloom, S., Xu, M., and Zambryski, P. C. (2011). Plasmodesmata during development: Re-examination of the importance of primary, secondary, and branched plasmodesmata structure versus function. *Protoplasma* 248. doi: 10.1007/s00709-010-0252-3

Burch-Smith, T. M., and Zambryski, P. C. (2010). Loss of increased size exclusion limit (ise)1 or ise2 increases the formation of secondary plasmodesmata. *Current Biology* 20. doi: 10.1016/j.cub.2010.03.064

Burkart, G. M., Baskin, T. I., and Bezanilla, M. (2015). A family of ROP proteins that suppresses actin dynamics, and is essential for polarized growth and cell adhesion. *J Cell*

Sci 128. doi: 10.1242/jcs.172445

Busch, H., Boerries, M., Bao, J., Hanke, S. T., Hiss, M., Tiko, T., et al. (2013). Network theory inspired analysis of time-resolved expression data reveals key players guiding *P. patens* stem cell development. *PLoS One* 8. doi: 10.1371/journal.pone.0060494

Buschmann, H., and Zachgo, S. (2016). The evolution of cell division: From Streptophyte algae to land plants. *Trends Plant Sci* 21. doi: 10.1016/j.tplants.2016.07.004

Cheng, X., Mwaura, B. W., Chang Stauffer, S. R., and Bezanilla, M. (2020). A fully functional ROP fluorescent fusion protein reveals roles for this GTPase in subcellular and tissue-level patterning. *Plant Cell* 32. doi: 10.1105/TPC.20.00440

Cilia, M. L., and Jackson, D. (2004). Plasmodesmata form and function. *Curr Opin Cell Biol* 16. doi: 10.1016/j.ceb.2004.08.002

Craddock, C., Lavagi, I., and Yang, Z. (2012). New insights into Rho signaling from plant ROP/Rac GTPases. *Trends Cell Biol* 22. doi: 10.1016/j.tcb.2012.05.002

Cutler, S. R., Rodriguez, P. L., Finkelstein, R. R., and Abrams, S. R. (2010). Abscisic acid: Emergence of a core signaling network. *Annu Rev Plant Biol* 61. doi: 10.1146/annurev-arplant-042809-112122

De Vries, J., Curtis, B. A., Gould, S. B., and Archibald, J. M. (2018). Embryophyte stress signaling evolved in the algal progenitors of land plants. *Proc Natl Acad Sci U S A* 115. doi: 10.1073/pnas.1719230115

Deeks, M. J., Hussey, P. J., and Davies, B. (2002). Formins: Intermediates in signal-transduction cascades that affect cytoskeletal reorganization. *Trends Plant Sci* 7. doi: 10.1016/S1360-1385(02)02341-5

Dünser, K., Gupta, S., Herger, A., Feraru, M. I., Ringli, C., and Kleine - Vehn, J. (2019). Extracellular matrix sensing by FERONIA and leucine - rich repeat extensins controls vacuolar expansion during cellular elongation in *Arabidopsis thaliana*. *EMBO J* 38. doi: 10.15252/embj.2018100353

Edgar, R. C. (2004). MUSCLE: Multiple sequence alignment with high accuracy and high throughput. *Nucleic Acids Res* 32. doi: 10.1093/nar/gkh340

Era, A., Tominaga, M., Ebine, K., Awai, C., Saito, C., Ishizaki, K., et al. (2009). Application of lifeact reveals F-actin dynamics in *Arabidopsis thaliana* and the liverwort, *Marchantia polymorpha*. *Plant Cell Physiol* 50. doi: 10.1093/pcp/pcp055

Evkaikina, A. I., Romanova, M. A., and Voitsekhovskaja, O. V. (2014). Evolutionary aspects of non-cell-autonomous regulation in vascular plants: Structural background and models to study. *Front Plant Sci* 5. doi: 10.3389/fpls.2014.00031

Feiguelman, G., Fu, Y., and Yalovsky, S. (2018). ROP GTPases structure-function and signaling pathways. *Plant Physiol* 176. doi: 10.1104/pp.17.01415

Fernandez-Calvino, L., Faulkner, C., Walshaw, J., Saalbach, G., Bayer, E., Benitez-Alfonso, Y., et al. (2011). *Arabidopsis* plasmodesmal proteome. *PLoS One* 6. doi: 10.1371/journal.pone.0018880

Firestone, G. L., and Kapadia, B. J. (2012). Minireview: Regulation of gap junction dynamics by nuclear hormone receptors and their ligands. *Molecular Endocrinology* 26. doi: 10.1210/me.2012-1065

Fitzgibbon, J., Beck, M., Zhou, J., Faulkner, C., Robatzek, S., and Oparka, K. (2013). A developmental framework for complex plasmodesmata formation revealed by large-scale imaging of the *Arabidopsis* leaf epidermis. *Plant Cell* 25. doi: 10.1105/tpc.112.105890

Furihata, T., Maruyama, K., Fujita, Y., Umezawa, T., Yoshida, R., Shinozaki, K., et al. (2006). Abscisic acid-dependent multisite phosphorylation regulates the activity of a transcription activator AREB1. *Proc Natl Acad Sci U S A* 103. doi: 10.1073/pnas.0505667103

Gombos, S., Miras, M., Howe, V., Xi, L., Pottier, M., Kazemein Jasemi, N. S., et al. (2023). A high-confidence *Physcomitrium patens* plasmodesmata proteome by iterative scoring and validation reveals diversification of cell wall proteins during evolution. *New Phytologist* 238, 637–653. doi: 10.1111/nph.18730

Graham, L. E., Cook, M. E., and Busse, J. S. (2000). The origin of plants: Body plan changes contributing to a major evolutionary radiation. *Proc Natl Acad Sci U S A* 97. doi: 10.1073/pnas.97.9.4535

Grosberg, R. K., and Strathmann, R. R. (2007). The evolution of multicellularity: A minor major transition? *Annu Rev Ecol Evol Syst* 38. doi: 10.1146/annurev.ecolsys.36.102403.114735

Grunt, M., Žárský, V., and Cvrčková, F. (2008). Roots of angiosperm formins: The evolutionary history of plant FH2 domain-containing proteins. *BMC Evol Biol* 8. doi: 10.1186/1471-2148-8-115

Gustafsson, N., Culley, S., Ashdown, G., Owen, D. M., Pereira, P. M., and Henriques, R. (2016). Fast live-cell conventional fluorophore nanoscopy with ImageJ through super-resolution radial fluctuations. *Nat Commun* 7. doi: 10.1038/ncomms12471

Han, X., Hyun, T. K., Zhang, M., Kumar, R., Koh, E. ji, Kang, B. H., et al. (2014). Auxin-callose-mediated plasmodesmal gating is essential for tropic auxin gradient formation and signaling. *Dev Cell* 28. doi: 10.1016/j.devcel.2013.12.008

Hepler, P. K. (1982). Endoplasmic reticulum in the formation of the cell plate and plasmodesmata. *Protoplasma* 111. doi: 10.1007/BF01282070

Hervé, J. C., and Derangeon, M. (2013). Gap-junction-mediated cell-to-cell communication. *Cell Tissue Res* 352. doi: 10.1007/s00441-012-1485-6

Hiroguchi, A., Nakamura, K., and Fujita, T. (2022). Abscisic acid switches cell division modes of asymmetric cell division and symmetric cell division in stem cells of protonemal filaments in the moss *Physcomitrium patens*. *Plant Biotechnology* 39. doi: 10.5511/plantbiotechnology.22.0107a

Hiwatashi, Y., Obara, M., Sato, Y., Fujita, T., Murata, T., and Hasebe, M. (2008). Kinesins are indispensable for interdigitation of phragmoplast microtubules in the moss *Physcomitrella patens*. *Plant Cell* 20. doi: 10.1105/tpc.108.061705

Hiwatashi, Y., Sato, Y., and Doonan, J. H. (2014). Kinesins have a dual function in organizing microtubules during both tip growth and cytokinesis in *Physcomitrella patens*. *Plant Cell* 26. doi: 10.1105/tpc.113.121723

Ito, K., Ren, J., and Fujita, T. (2014). Conserved function of Rho-related Rop/RAC GTPase signaling in regulation of cell polarity in *Physcomitrella patens*. *Gene* 544. doi: 10.1016/j.gene.2014.04.057

Jaffe, A. B., and Hall, A. (2005). Rho GTPases: Biochemistry and biology. *Annu Rev Cell Dev Biol* 21. doi: 10.1146/annurev.cellbio.21.020604.150721

Jedd, G., and Chua, N. H. (2000). A new self-assembled peroxisomal vesicle required for efficient resealing of the plasma membrane. *Nat Cell Biol* 2. doi: 10.1038/35008652

Johnston, M. G., Breakspear, A., Samwald, S., Zhang, D., Papp, D., Faulkner, C., et al. (2023). Comparative phyloproteomics identifies conserved plasmodesmal proteins. *J Exp Bot* 74, 1821–1835. doi: 10.1093/jxb/erad022

Khandelwal, A., Cho, S. H., Marella, H., Sakata, Y., Perroud, P. F., Pan, A., et al. (2010). Role of ABA and ABI3 in desiccation tolerance. *Science (1979)* 327. doi: 10.1126/science.1183672

Kitagawa, M., and Fujita, T. (2013). Quantitative imaging of directional transport through plasmodesmata in moss protonemata via single-cell photoconversion of Dendra2. *J Plant Res* 126. doi: 10.1007/s10265-013-0547-5

Kitagawa, M., and Fujita, T. (2015). A model system for analyzing intercellular communication through plasmodesmata using moss protonemata and leaves. *J Plant Res* 128. doi: 10.1007/s10265-014-0690-7

Kitagawa, M., Tomoi, T., Fukushima, T., Sakata, Y., Sato, M., Toyooka, K., et al. (2019). Abscisic acid acts as a regulator of molecular trafficking through plasmodesmata in the moss *Physcomitrella patens*. *Plant Cell Physiol* 60. doi: 10.1093/pcp/pcy249

Knoll, A. H. (2011). The multiple origins of complex multicellularity. *Annu Rev Earth Planet Sci* 39. doi: 10.1146/annurev.earth.031208.100209

Kofuji, R., and Hasebe, M. (2014). Eight types of stem cells in the life cycle of the moss *Physcomitrella patens*. *Curr Opin Plant Biol* 17. doi: 10.1016/j.pbi.2013.10.007

Komatsu, K., Suzuki, N., Kuwamura, M., Nishikawa, Y., Nakatani, M., Ohtawa, H., et al. (2013). Group A PP2Cs evolved in land plants as key regulators of intrinsic desiccation tolerance. *Nat Commun* 4. doi: 10.1038/ncomms3219

Komatsu, K., Takezawa, D., and Sakata, Y. (2020). Decoding ABA and osmostress signalling in plants from an evolutionary point of view. in *Plant Cell and Environment*. doi: 10.1111/pce.13869

Kost, B., Lemichez, E., Spielhofer, P., Hong, Y., Tolias, K., Carpenter, C., et al. (2000). Rac homologues and compartmentalized phosphatidylinositol 4,5- bisphosphate act in a common pathway to regulate polar pollen tube growth. *Journal of Cell Biology* 145. doi: 10.1083/jcb.145.2.317

Kraner, M. E., Link, K., Melzer, M., Ekici, A. B., Uebe, S., Tarazona, P., et al. (2017). Choline transporter-like1 (CHER1) is crucial for plasmodesmata maturation in *Arabidopsis thaliana*. *Plant Journal* 89, 394–406. doi: 10.1111/tpj.13393

Krüger, F., and Schumacher, K. (2018). Pumping up the volume – vacuole biogenesis in *Arabidopsis thaliana*. *Semin Cell Dev Biol* 80. doi: 10.1016/j.semcdb.2017.07.008

Kühn, S., and Geyer, M. (2014). Formins as effector proteins of rho GTPases. *Small GTPases* 5. doi: 10.4161/sgtp.29513

Kurotani, K. I., and Notaguchi, M. (2021). Cell-to-cell connection in plant grafting—molecular insights into symplasmic reconstruction. *Plant Cell Physiol* 62. doi: 10.1093/pcp/pcab109

Leader, B., Lim, H., Carabatsos, M. J., Harrington, A., Ecsedy, J., Pellman, D., et al. (2002). Formin-2, polyploidy, hypofertility and positioning of the meiotic spindle in mouse oocytes. *Nat Cell Biol* 4. doi: 10.1038/ncb880

Lee, R. E. (1971). The pit connections of some lower red algae: Ultrastructure and phylogenetic significance. *British Phycological Journal* 6. doi: 10.1080/00071617100650031

Lemichez, E., Wu, Y., Sanchez, J. P., Mettouchi, A., Mathur, J., and Chua, N. H. (2001). Inactivation of AtRac1 by abscisic acid is essential for stomatal closure. *Genes Dev* 15. doi: 10.1101/gad.900401

Levy, A., Erlanger, M., Rosenthal, M., and Epel, B. L. (2007). A plasmodesmata-associated β-1,3-glucanase in *Arabidopsis*. *Plant Journal* 49, 669–682. doi: 10.1111/j.1365-313X.2006.02986.x

Li, Z., Li, Z., Gao, X., Chinnusamy, V., Bressan, R., Wang, Z. X., et al. (2012). ROP11 GTPase negatively regulates ABA signaling by protecting ABI1 phosphatase activity from inhibition by the ABA receptor RCAR1/PYL9 in *Arabidopsis*. *J Integr Plant Biol* 54. doi: 10.1111/j.1744-7909.2012.01101.x

Li, Z., Waadt, R., and Schroeder, J. I. (2016). Release of GTP exchange factor mediated down-regulation of abscisic acid signal transduction through ABA-induced rapid degradation of RopGEFs. *PLoS Biol* 14. doi: 10.1371/journal.pbio.1002461

Lin, Y., and Yang, Z. (1997). Inhibition of pollen tube elongation by microinjected anti-Rop1Ps antibodies suggests a crucial role for Rho-type GTPases in the control of tip growth. *Plant Cell* 9. doi: 10.1105/tpc.9.9.1647

López-Sáez, J. F., Giménez-Martin, G., and Risueño, M. C. (1966). Fine structure of the plasmodesm. *Protoplasma* 61. doi: 10.1007/BF01247912

McLean, B. G., Hempel, F. D., and Zambryski, P. C. (1997). Plant intercellular communication via plasmodesmata. *Plant Cell* 9. doi: 10.1105/tpc.9.7.1043

Mohanasundaram, B., Bhide, A. J., Palit, S., Chaturvedi, G., Lingwan, M., Masakapalli, S. K., et al. (2021). The unique bryophyte-specific repeat-containing protein SHORT-LEAF regulates gametophore development in moss. *Plant Physiol* 187, 203–217. doi: 10.1093/plphys/kiab261

Muller, A., Fujita, T., and Coudert, Y. (2022). "Callose detection and quantification at plasmodesmata in Bryophytes," in *Methods in Molecular Biology* , 177–187. doi: 10.1007/978-1-0716-2132-5_11

Nakashima, K., Fujita, Y., Kanamori, N., Katagiri, T., Umezawa, T., Kidokoro, S., et al. (2009). Three *Arabidopsis* SnRK2 protein kinases, SRK2D/SnRK2.2, SRK2E/SnRK2.6/OST1 and SRK2I/SnRK2.3, involved in ABA signaling are essential for the control of seed development and dormancy. *Plant Cell Physiol* 50. doi: 10.1093/pcp/pcp083

Nicolas, W. J., Grison, M. S., and Bayer, E. M. (2017). Shaping intercellular channels of plasmodesmata: The structure-to-function missing link. *J Exp Bot* 69. doi: 10.1093/jxb/erx225

Nishiyama, T. (2000). Tagged mutagenesis and gene-trap in the moss, *Physcomitrella patens* by shuttle mutagenesis. *DNA Research* 7, 9–17. doi: 10.1093/dnares/7.1.9

Oda, Y., and Fukuda, H. (2012). Initiation of cell wall pattern by a Rho- and microtubule-driven symmetry breaking. *Science (1979)* 337. doi: 10.1126/science.1222597

Oda, Y., Hirata, A., Sano, T., Fujita, T., Hiwatashi, Y., Sato, Y., et al. (2009). Microtubules regulate dynamic organization of vacuoles in *Physcomitrella patens*. *Plant Cell Physiol* 50. doi: 10.1093/pcp/pcp031

Ormenese, S., Bernier, G., and Périlleux, C. (2006). Cytokinin application to the shoot apical meristem of *Sinapis alba* enhances secondary plasmodesmata formation. *Planta* 224. doi: 10.1007/s00425-006-0317-x

Park, S. Y., Fung, P., Nishimura, N., Jensen, D. R., Fujii, H., Zhao, Y., et al. (2009). Abscisic acid inhibits type 2C protein phosphatases via the PYR/PYL family of START proteins.

Science (1979) 324. doi: 10.1126/science.1173041

PORTER, K. R., and MACHADO, R. D. (1960). Studies on the endoplasmic reticulum. IV. Its form and distribution during mitosis in cells of onion root tip. *J Biophys Biochem Cytol* 7. doi: 10.1083/jcb.7.1.167

Radford, J. E., Vesk, M., and Overall, R. L. (1998). Callose deposition at plasmodesmata. *Protoplasma* 201. doi: 10.1007/BF01280708

Rappel, W. J., and Edelstein-Keshet, L. (2017). Mechanisms of cell polarization. *Curr Opin Syst Biol* 3. doi: 10.1016/j.coisb.2017.03.005

Rensing, S. A., Goffinet, B., Meyberg, R., Wu, S. Z., and Bezanilla, M. (2020). The moss *Physcomitrium* (*Physcomitrella*) *patens*: A model organism for non-seed plants. *Plant Cell* 32. doi: 10.1105/tpc.19.00828

Robards, A. W. (1976). "Plasmodesmata in higher plants," in *Intercellular Communication in Plants: Studies on Plasmodesmata* (Berlin, Heidelberg: Springer Berlin Heidelberg), 15–57. doi: 10.1007/978-3-642-66294-2_2

Ruan, J., Lai, L., Ou, H., and Yi, P. (2023). Two subtypes of GTPase-activating proteins coordinate tip growth and cell size regulation in *Physcomitrium patens*. *Nat Commun* 14, 7084. doi: 10.1038/s41467-023-42879-y

Rustom, A., Saffrich, R., Markovic, I., Walther, P., and Gerdes, H. H. (2004). Nanotubular highways for intercellular organelle transport. *Science (1979)* 303. doi: 10.1126/science.1093133

Sager, R. E., and Lee, J.-Y. (2018). Plasmodesmata at a glance. *J Cell Sci* 131. doi: 10.1242/jcs.209346

Sager, R., and Lee, J. Y. (2014). Plasmodesmata in integrated cell signalling: Insights from development and environmental signals and stresses. *J Exp Bot* 65. doi: 10.1093/jxb/eru365

Sakai, Y., Higaki, T., Ishizaki, K., Nishihama, R., Kohchi, T., and Hasezawa, S. (2022). Migration of prospindle before the first asymmetric divisioin in germinating spore of *Marchantia polymorpha*. *Plant Biotechnology* 39. doi: 10.5511/plantbiotechnology.21.1217b

Salmon, M. S., and Bayer, E. M. F. (2013). Dissecting plasmodesmata molecular composition by mass spectrometry-based proteomics. *Front Plant Sci* 3. doi: 10.3389/fpls.2012.00307

Sankoh, A. F., and Burch-Smith, T. M. (2021). Plasmodesmata and hormones: pathways for plant development. *Am J Bot* 108. doi: 10.1002/ajb2.1733

Schindelin, J., Arganda-Carreras, I., Frise, E., Kaynig, V., Longair, M., Pietzsch, T., et al. (2012). Fiji: An open-source platform for biological-image analysis. *Nat Methods* 9. doi:

10.1038/nmeth.2019

Schnepf, E., and Reinhard, C. (1997). Brachycytes in *Funaria* protonemate: Induction by abscisic acid and fine structure. *J Plant Physiol* 151. doi: 10.1016/S0176-1617(97)80149-6

Segretain, D., and Falk, M. M. (2004). Regulation of connexin biosynthesis, assembly, gap junction formation, and removal. *Biochim Biophys Acta Biomembr* 1662. doi: 10.1016/j.bbamem.2004.01.007

Seguí-Simarro, J. M., and Staehelin, L. A. (2006). Cell cycle-dependent changes in golgi stacks, vacuoles, clathrin-coated vesicles and multivesicular bodies in meristematic cells of *Arabidopsis thaliana*: A quantitative and spatial analysis. *Planta* 223. doi: 10.1007/s00425-005-0082-2

Shinozawa, A., Otake, R., Takezawa, D., Umezawa, T., Komatsu, K., Tanaka, K., et al. (2019). SnRK2 protein kinases represent an ancient system in plants for adaptation to a terrestrial environment. *Commun Biol* 2. doi: 10.1038/s42003-019-0281-1

Skubacz, A., Daszkowska-Golec, A., and Szarejko, I. (2016). The role and regulation of ABI5 (ABA-insensitive 5) in plant development, abiotic stress responses and phytohormone crosstalk. *Front Plant Sci* 7. doi: 10.3389/fpls.2016.01884

Smokvarska, M., Francis, C., Platre, M. P., Fiche, J. B., Alcon, C., Dumont, X., et al. (2020). A plasma membrane nanodomain ensures signal specificity during osmotic signaling in plants. *Current Biology* 30. doi: 10.1016/j.cub.2020.09.013

Smokvarska, M., Jaillais, Y., and Martiniere, A. (2021). Function of membrane domains in rho-of-plant signaling. *Plant Physiol* 185. doi: 10.1093/PLPHYS/KIAA082

Söhl, G., and Willecke, K. (2004). Gap junctions and the connexin protein family. *Cardiovasc Res* 62. doi: 10.1016/j.cardiores.2003.11.013

Sorek, N., Gutman, O., Bar, E., Abu-Abied, M., Feng, X., Running, M. P., et al. (2011). Differential effects of prenylation and S-acylation on type I and II ROPS membrane interaction and function. *Plant Physiol* 155. doi: 10.1104/pp.110.166850

Staps, M., van Gestel, J., and Tarnita, C. E. (2019). Emergence of diverse life cycles and life histories at the origin of multicellularity. *Nat Ecol Evol* 3. doi: 10.1038/s41559-019-0940-0

Steinberg, G., Peñalva, M. A., Riquelme, M., Wösten, H. A., and Harris, S. D. (2017). Cell biology of hyphal growth. *Microbiol Spectr* 5. doi: 10.1128/microbiolspec.funk-0034-2016

Sun, Y., Harpazi, B., Wijerathna-Yapa, A., Merilo, E., de Vries, J., Michaeli, D., et al. (2019). A ligand-independent origin of abscisic acid perception. *Proc Natl Acad Sci U S A* 116. doi: 10.1073/pnas.1914480116

Sun, Y., Pri-Tal, O., Michaeli, D., and Mosquna, A. (2020). Evolution of abscisic acid signaling module and its perception. *Front Plant Sci* 11. doi: 10.3389/fpls.2020.00934

Tajbakhsh, S., Rocheteau, P., and Le Roux, I. (2009). Asymmetric cell divisions and asymmetric cell fates. *Annu Rev Cell Dev Biol* 25. doi: 10.1146/annurev.cellbio.24.110707.175415

Terauchi, M., Nagasato, C., and Motomura, T. (2015). Plasmodesmata of brown algae. *J Plant Res* 128. doi: 10.1007/s10265-014-0677-4

Thelander, M., Olsson, T., and Ronne, H. (2005). Effect of the energy supply on filamentous growth and development in *Physcomitrella patens*. *J Exp Bot* 56. doi: 10.1093/jxb/eri040

Thole, J. M., Perroud, P. F., Quatrano, R. S., and Running, M. P. (2014). Prenylation is required for polar cell elongation, cell adhesion, and differentiation in *Physcomitrella patens*. *Plant Journal* 78. doi: 10.1111/tpj.12484

Tilsner, J., Nicolas, W., Rosado, A., and Bayer, E. M. (2016). Staying tight: plasmodesmal membrane contact sites and the control of cell-to-cell connectivity in plants. *Annu Rev Plant Biol* 67. doi: 10.1146/annurev-arplant-043015-111840

Tomoi, T., Kawade, K., Kitagawa, M., Sakata, Y., Tsukaya, H., and Fujita, T. (2020). Quantitative imaging reveals distinct contributions of SnRK2 and ABI3 in plasmodesmatal permeability in *Physcomitrella patens*. *Plant Cell Physiol* 61. doi: 10.1093/pcp/pcaa021

Toriyama, T., Shinozawa, A., Yasumura, Y., Saruhashi, M., Hiraide, M., Ito, S., et al. (2022). Sensor histidine kinases mediate ABA and osmostress signaling in the moss *Physcomitrium patens*. *Current Biology* 32, 164-175.e8. doi: 10.1016/j.cub.2021.10.068

Treuner-Lange, A., and Søgaard-Andersen, L. (2014). Regulation of cell polarity in bacteria. *Journal of Cell Biology* 206. doi: 10.1083/jcb.201403136

Tukey, J. W. (1949). Comparing individual means in the analysis of variance. *Biometrics* 5. doi: 10.2307/3001913

Tylewicz, S., Petterle, A., Marttila, S., Miskolczi, P., Azeez, A., Singh, R. K., et al. (2018). Photoperiodic control of seasonal growth is mediated by ABA acting on cell-cell communication. *Science (1979)* 360, 212–215. doi: 10.1126/science.aan8576

Ueda, M., Zhang, Z., and Laux, T. (2011). Transcriptional activation of *Arabidopsis* axis patterning genes WOX8/9 links zygote polarity to embryo development. *Dev Cell* 20. doi: 10.1016/j.devcel.2011.01.009

Umezawa, T., Sugiyama, N., Takahashi, F., Anderson, J. C., Ishihama, Y., Peck, S. C., et al. (2013). Genetics and phosphoproteomics reveal a protein phosphorylation network in the abscisic acid signaling pathway in *Arabidopsis thaliana*. *Sci Signal* 6. doi:

10.1126/scisignal.2003509

van Gisbergen, P. A. C., Li, M., Wu, S. Z., and Bezanilla, M. (2012). Class II formin targeting to the cell cortex by binding PI(3,5)P 2 is essential for polarized growth. *Journal of Cell Biology* 198. doi: 10.1083/jcb.201112085

Van Gisbergen, P., Wu, S. Z., Cheng, X., Pattavina, K. A., and Bezanilla, M. (2020). In vivo analysis of formin dynamics in the moss *P. patens* reveals functional class diversification. *J Cell Sci* 133. doi: 10.1242/jcs.233791

Vatén, A., Dettmer, J., Wu, S., Stierhof, Y. D., Miyashima, S., Yadav, S. R., et al. (2011). Callose biosynthesis regulates symplastic trafficking during root development. *Dev Cell* 21. doi: 10.1016/j.devcel.2011.10.006

Vidali, L., Van Gisbergen, P. A. C., Guérin, C., Franco, P., Li, M., Burkart, G. M., et al. (2009). Rapid formin-mediated actin-filament elongation is essential for polarized plant cell growth. *Proc Natl Acad Sci U S A* 106. doi: 10.1073/pnas.0901170106

Wang, H., Zhuang, X., Cai, Y., Cheung, A. Y., and Jiang, L. (2013a). Apical F-actin-regulated exocytic targeting of NtPPME1 is essential for construction and rigidity of the pollen tube cell wall. *Plant Journal* 76. doi: 10.1111/tpj.12300

Wang, Y., Li, L., Ye, T., Lu, Y., Chen, X., and Wu, Y. (2013b). The inhibitory effect of ABA on floral transition is mediated by ABI5 in *Arabidopsis*. *J Exp Bot* 64. doi: 10.1093/jxb/ers361

Wegner, L., Porth, M. L., and Ehlers, K. (2023). Multicellularity and the need for communication—a systematic overview on (algal) Plasmodesmata and other types of symplasmic cell connections. *Plants* 12. doi: 10.3390/plants12183342

Welch, B. L. (1938). The significance of the difference between two means when the population variances are unequal. *Biometrika* 29. doi: 10.2307/2332010

Wu, J.-I., and Wang, L.-H. (2019). Emerging roles of gap junction proteins connexins in cancer metastasis, chemoresistance and clinical application. *J Biomed Sci* 26, 8. doi: 10.1186/s12929-019-0497-x

Wu, S. Z., and Bezanilla, M. (2018). Actin and microtubule cross talk mediates persistent polarized growth. *Journal of Cell Biology* 217. doi: 10.1083/JCB.201802039

Xu, M., Cho, E., Burch-Smith, T. M., and Zambryski, P. C. (2012). Plasmodesmata formation and cell-to-cell transport are reduced in decreased size exclusion limit 1 during embryogenesis in *Arabidopsis*. *Proc Natl Acad Sci U S A* 109. doi: 10.1073/pnas.1202919109

Yamada, M., and Goshima, G. (2017). Mitotic spindle assembly in land plants: Molecules and mechanisms. *Biology (Basel)* 6. doi: 10.3390/biology6010006

Yang, Y., Xie, X., Tao, S., Zhou, K., Yu, Y., Lu, Z., et al. (2020). Plasmodesmata play a critical

role in promoting the germination of floral buds in *Ilex verticillata*. *Plant Growth Regul* 91, 349–357. doi: 10.1007/s10725-020-00609-0

Yi, P., and Goshima, G. (2020). Rho of plants GTPases and cytoskeletal elements control nuclear positioning and asymmetric cell division during *Physcomitrella patens* branching. *Current Biology* 30. doi: 10.1016/j.cub.2020.05.022

Yong, J. L., Szumlanski, A., Nielsen, E., and Yang, Z. (2008). Rho-GTPase-dependent filamentous actin dynamics coordinate vesicle targeting and exocytosis during tip growth. *Journal of Cell Biology* 181. doi: 10.1083/jcb.200801086

Zavaliev, R., Ueki, S., Epel, B. L., and Citovsky, V. (2011). Biology of callose (β -1,3-glucan) turnover at plasmodesmata. *Protoplasma* 248. doi: 10.1007/s00709-010-0247-0

Zhao, M., Li, Q., Chen, Z., Lv, Q., Bao, F., Wang, X., et al. (2018a). Regulatory mechanism of ABA and ABI3 on vegetative development in the moss *Physcomitrella patens*. *Int J Mol Sci* 19. doi: 10.3390/ijms19092728

Zhao, Y., Zhang, Z., Gao, J., Wang, P., Hu, T., Wang, Z., et al. (2018b). *Arabidopsis* duodecuple mutant of PYL ABA receptors reveals PYL repression of ABA-independent SnRK2 activity. *Cell Rep* 23, 3340-3351.e5. doi: 10.1016/j.celrep.2018.05.044

Zheng, Z. L., Nafisi, M., Tam, A., Li, H., Crowell, D. N., Narasimha Chary, S., et al. (2002). Plasma membrane-associated rop10 small GTPase is a specific negative regulator of abscisic acid responses in *Arabidopsis*. *Plant Cell* 14. doi: 10.1105/tpc.005611

Zheng, Z. L., and Yang, Z. (2000). The Rop GTPase: An emerging signaling switch in plants. *Plant Mol Biol* 44. doi: 10.1023/A:1006402628948

Zhu, T., Lucas, W. J., and Rost, T. L. (1998). Directional cell-to-cell communication in the *Arabidopsis* root apical meristem I. An ultrastructural and functional analysis. *Protoplasma* 203, 35–47. doi: 10.1007/BF01280585

Graphical overview of this dissertation

General introduction: Multicellularity and cell-to-cell communication

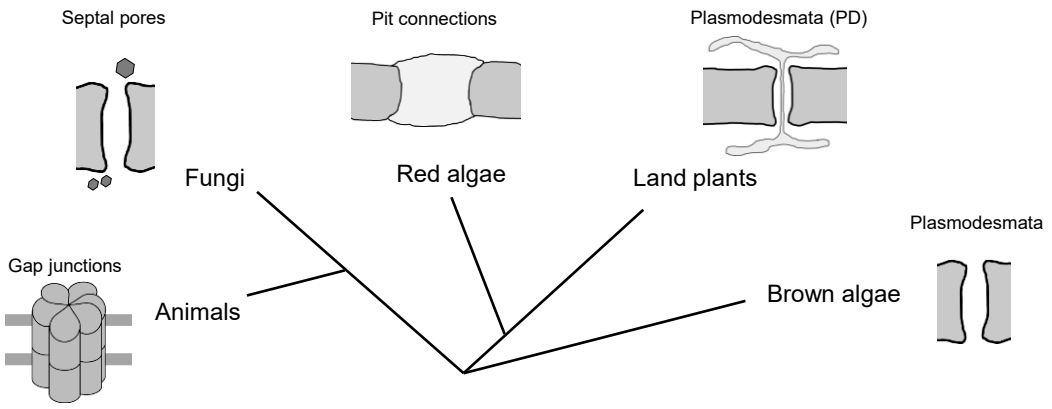

Analysis of cell types and mutants with disrupted multicellular body plan in protonema of *P. patens*

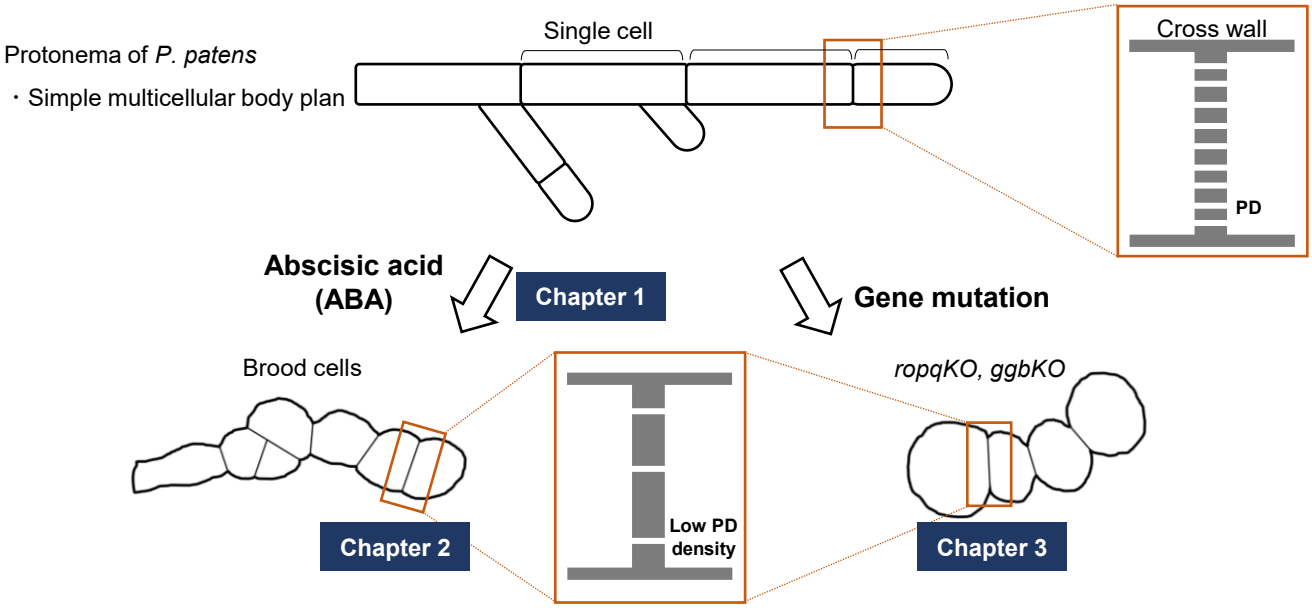

Chapter 1; Morphological changes in brood cell formation

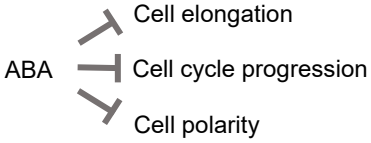

Chapter 2; ABA decreases PD density in brood cell formation

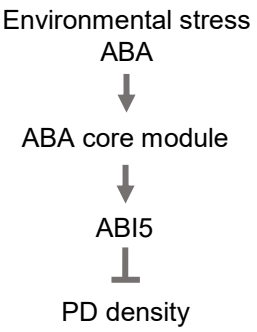

Chapter 3; ROP signaling is important for PD formation

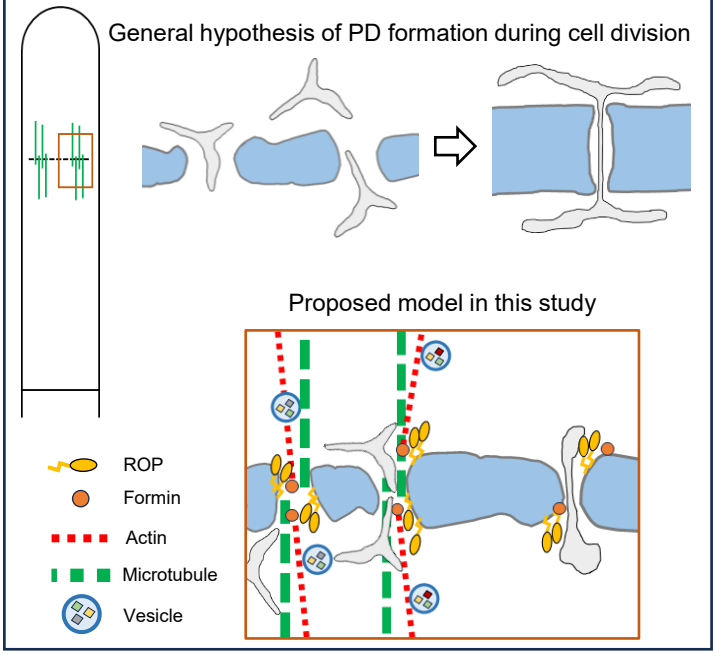

Chapter 1; Figure 1

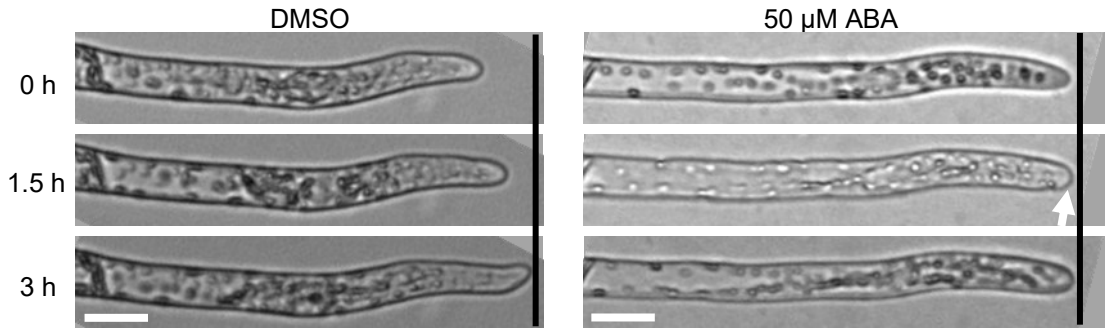

Chapter 1; Figure 2

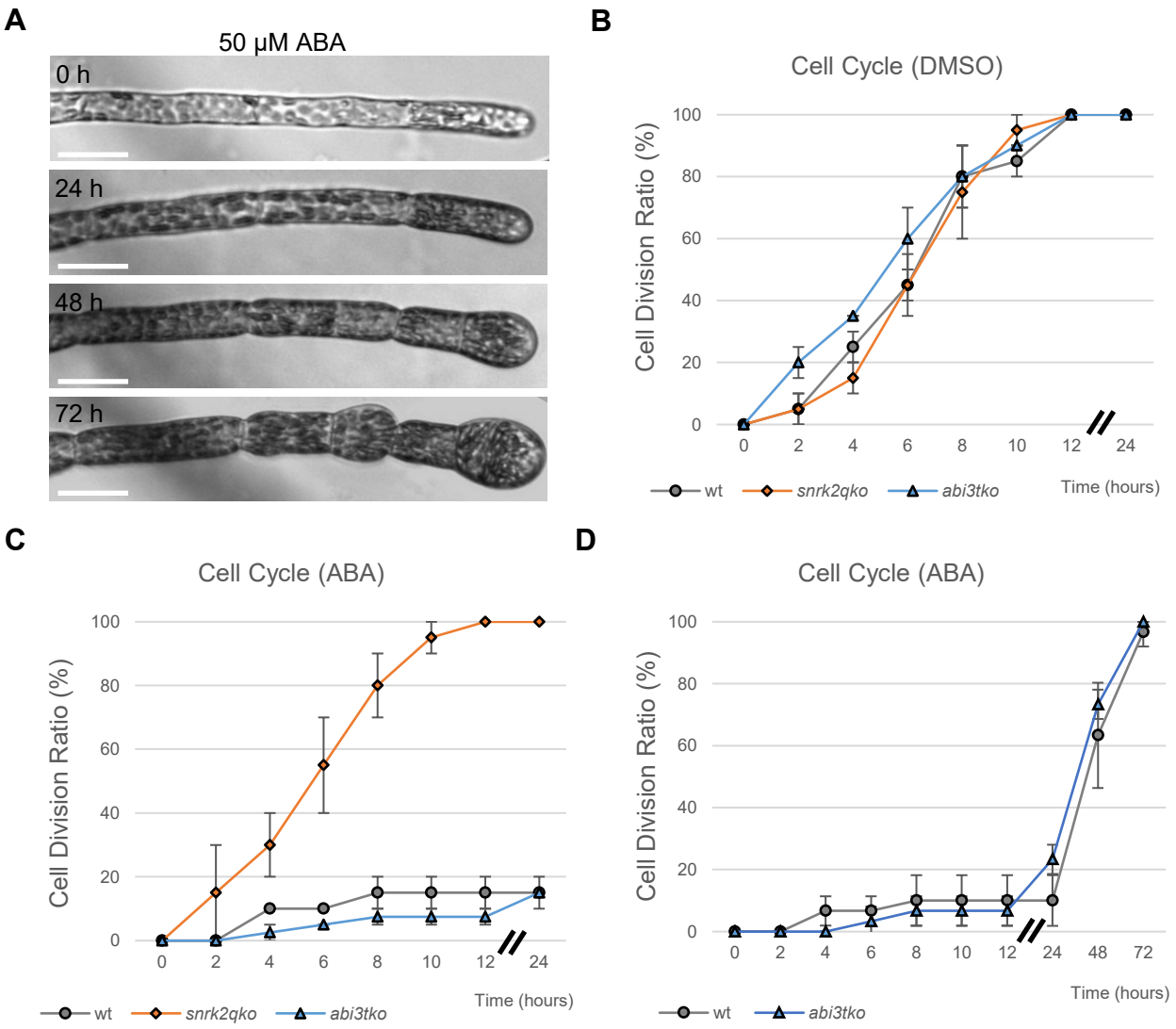

Chapter 1; Figure 3

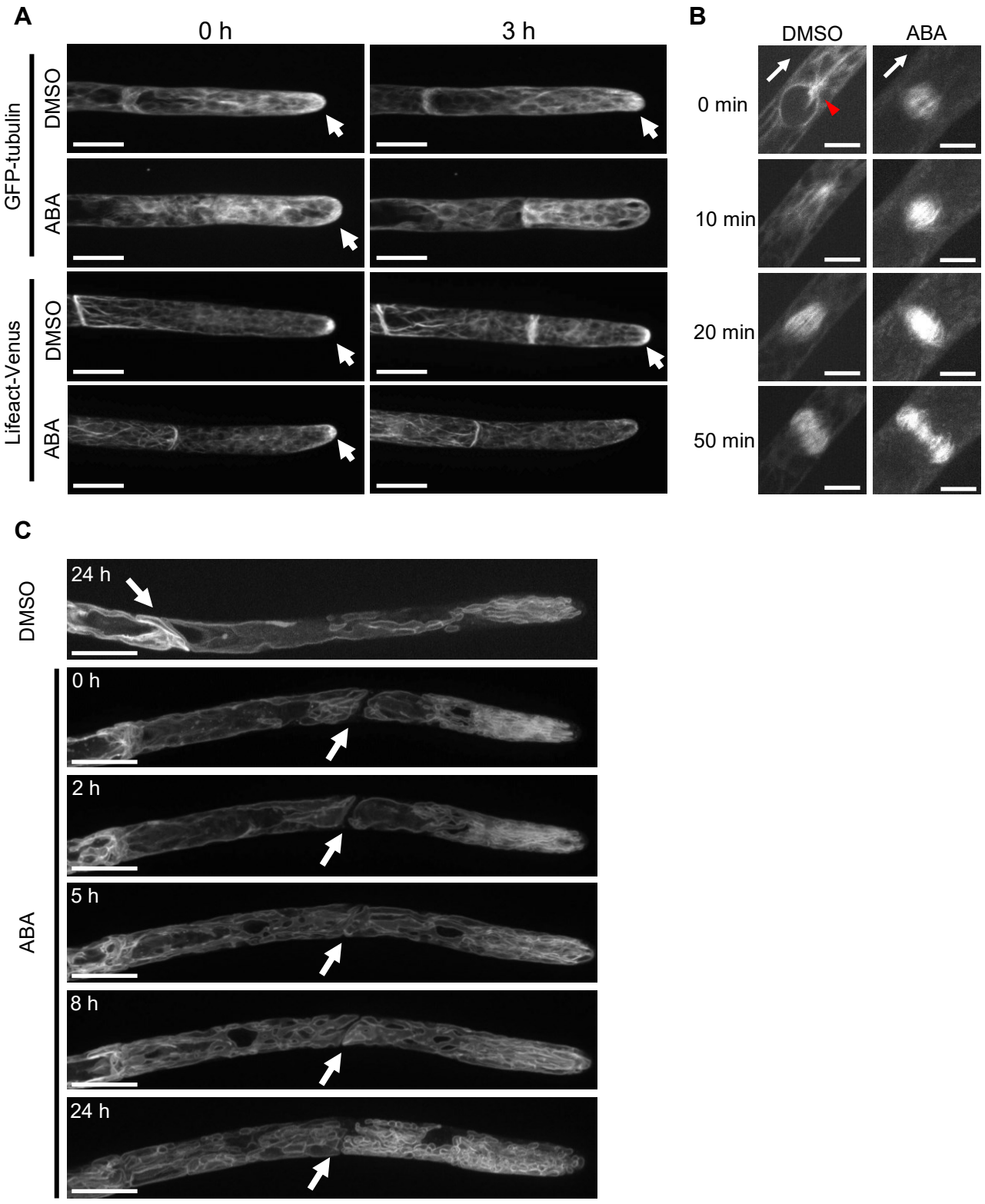

Chapter 2; Figure 1

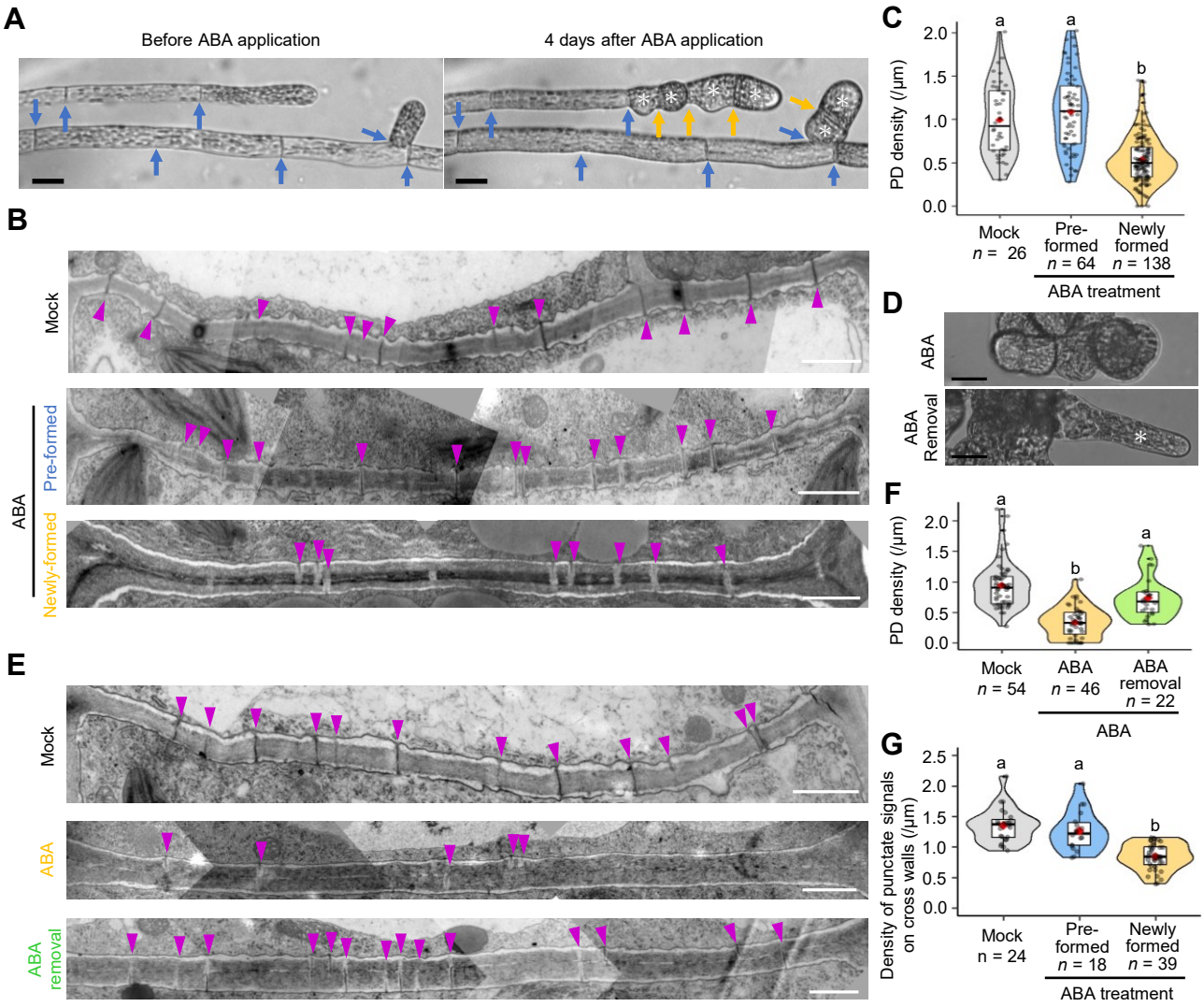

Chapter 2; Figure 2

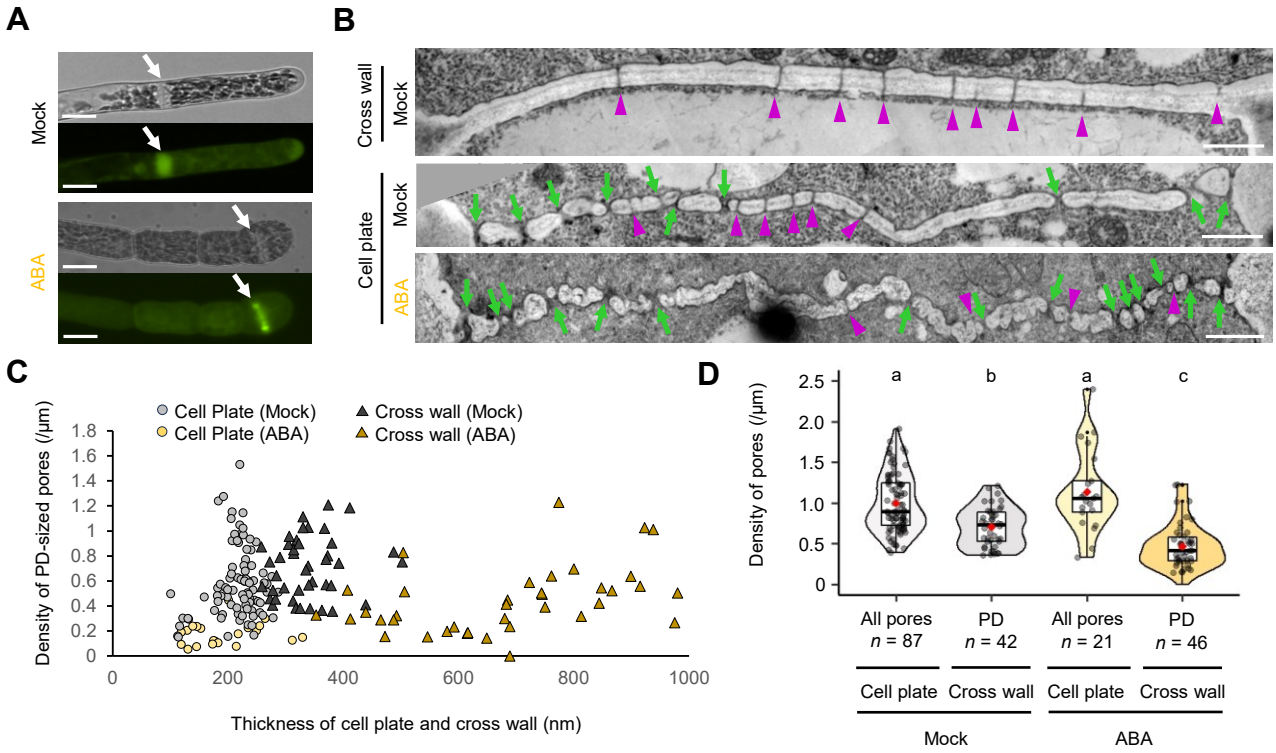

Chapter 2; Figure 3

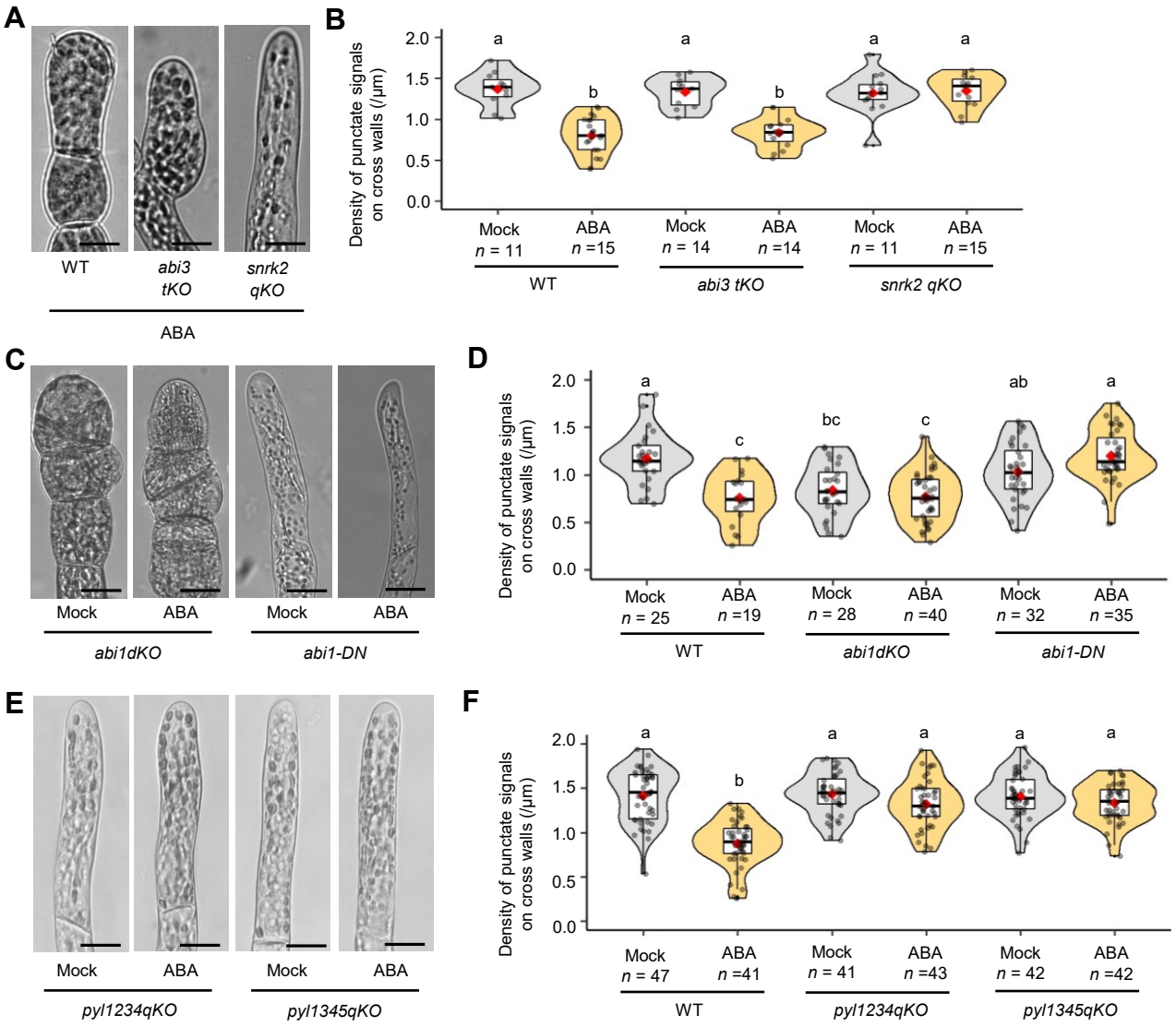

Chapter 2; Figure 4

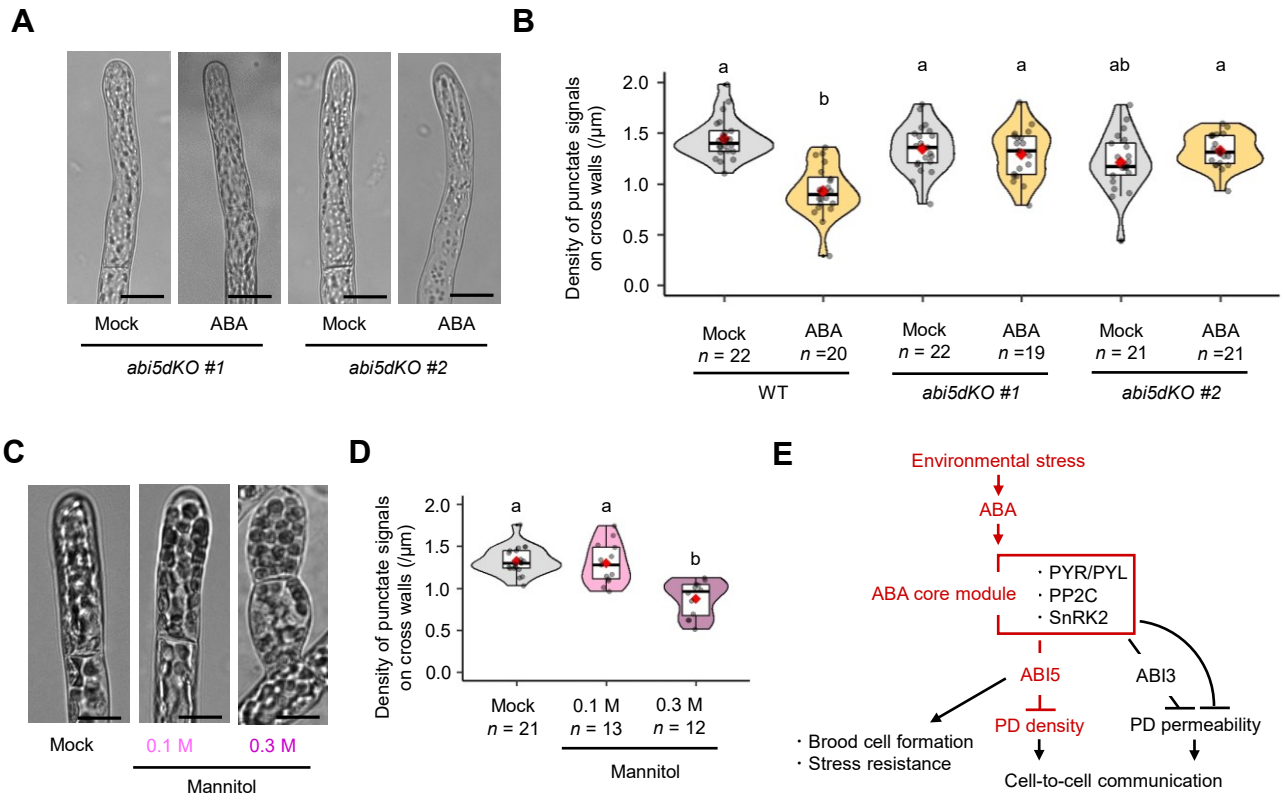

Chapter 2; Supplementary Figure S1

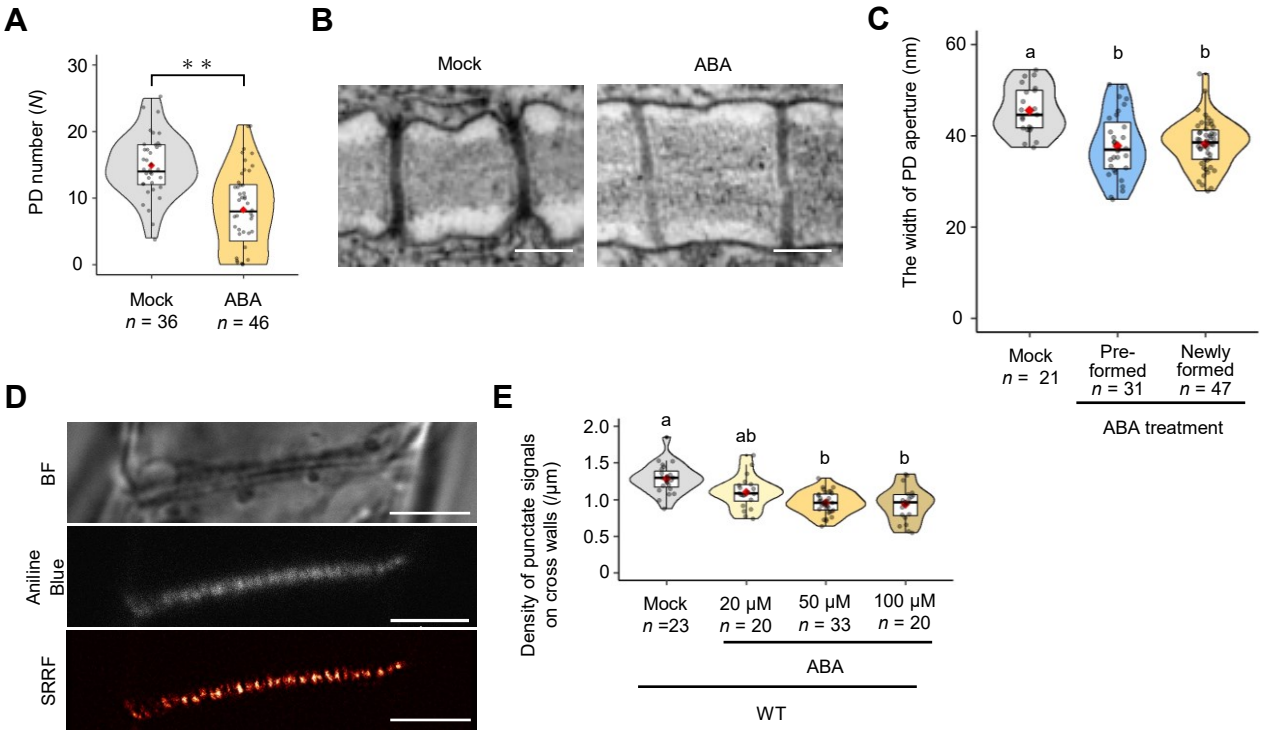

Chapter 2; Supplementary Figure S2

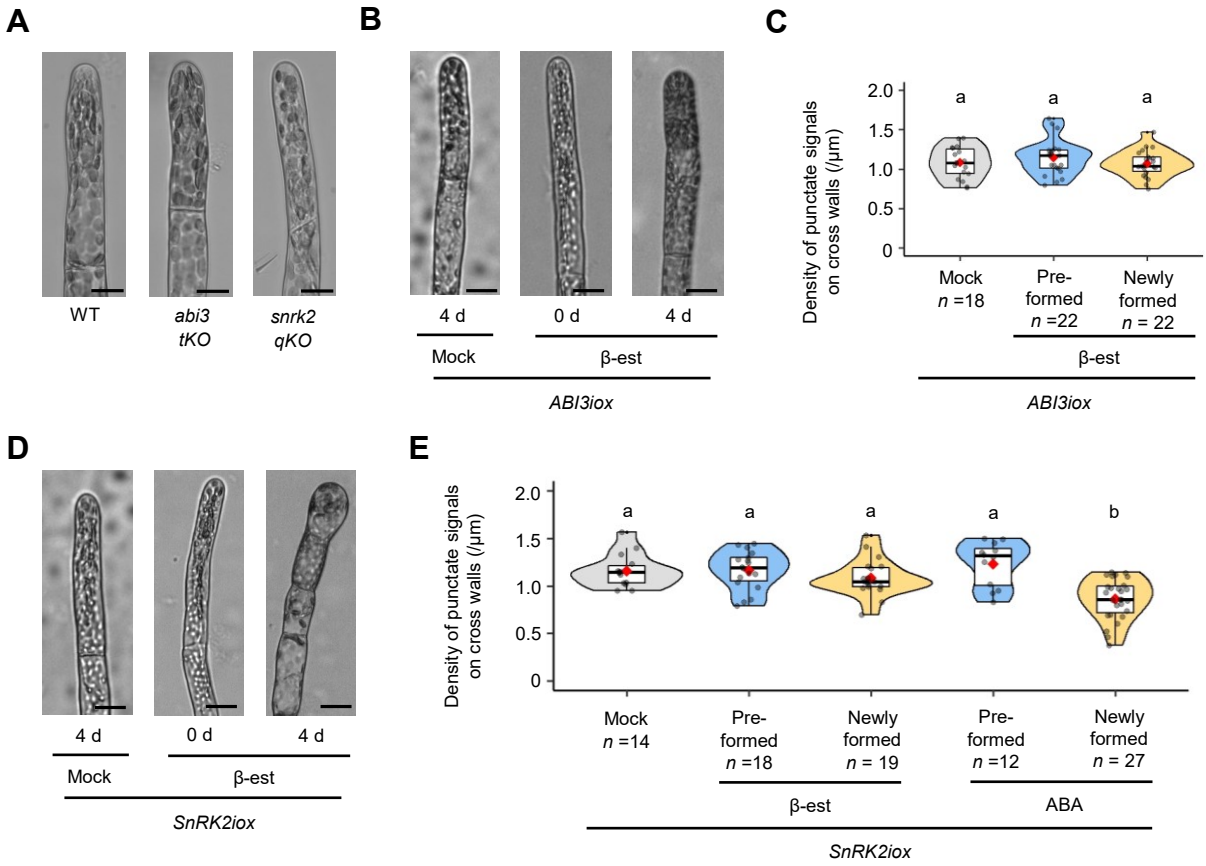

Chapter 2; Supplementary Figure S3

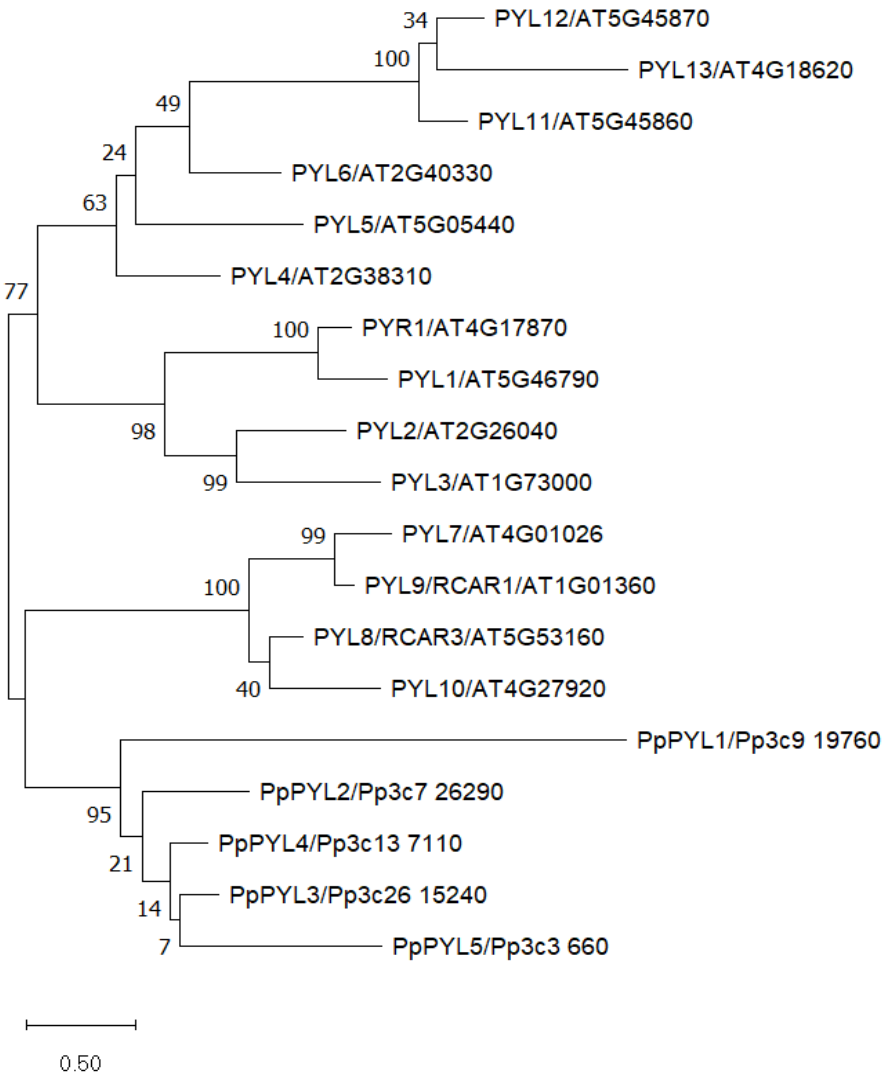

Chapter 2; Supplementary Figure S4

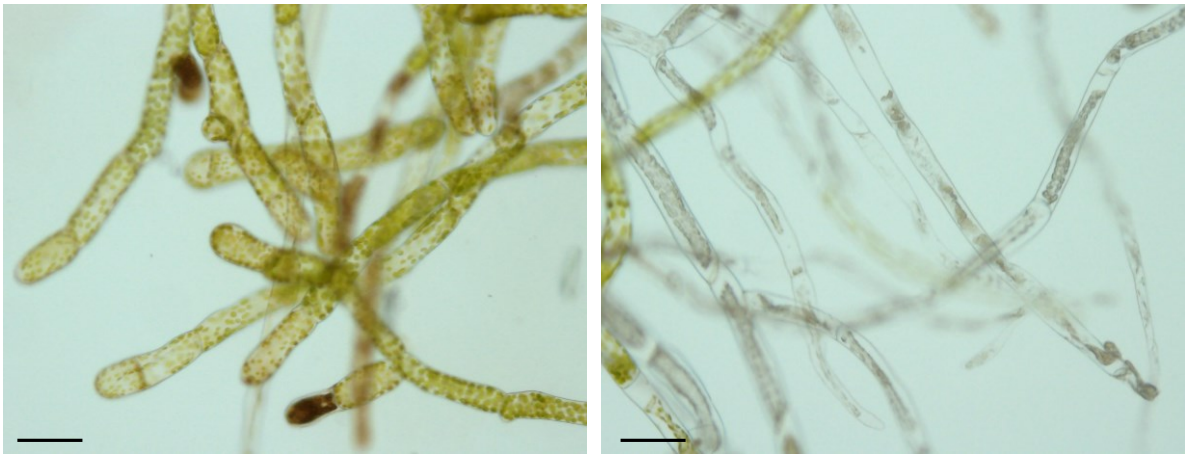

WT *snrk2qKO*

Chapter 3; Figure 1

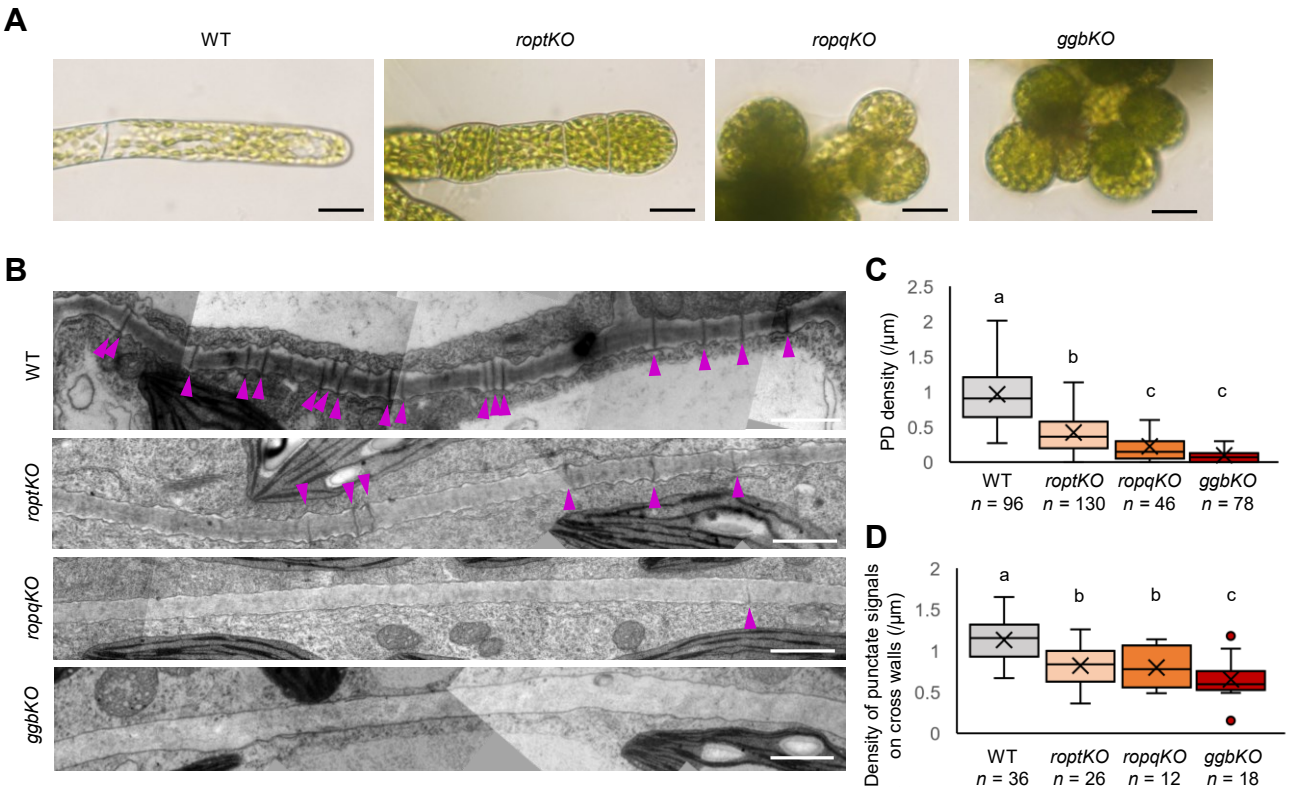

Chapter 3; Figure 2

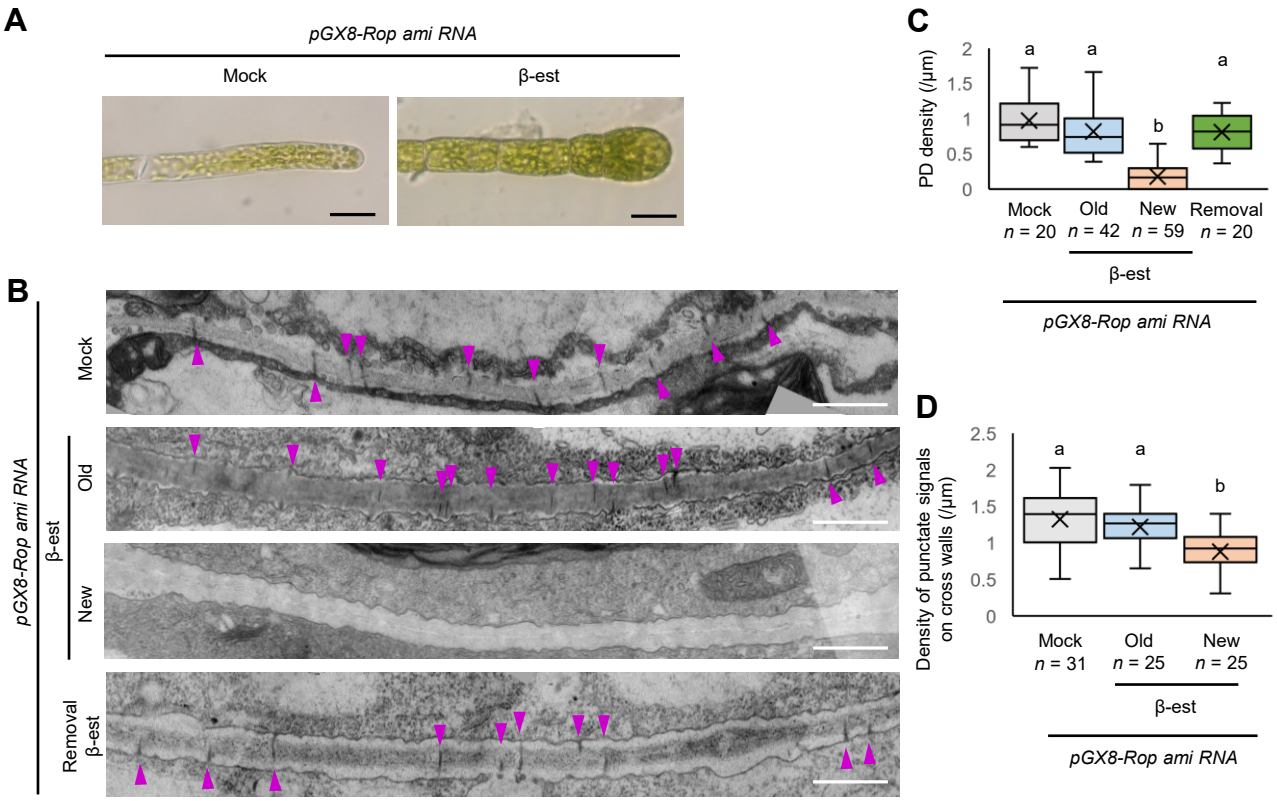

Chapter 3; Figure 3

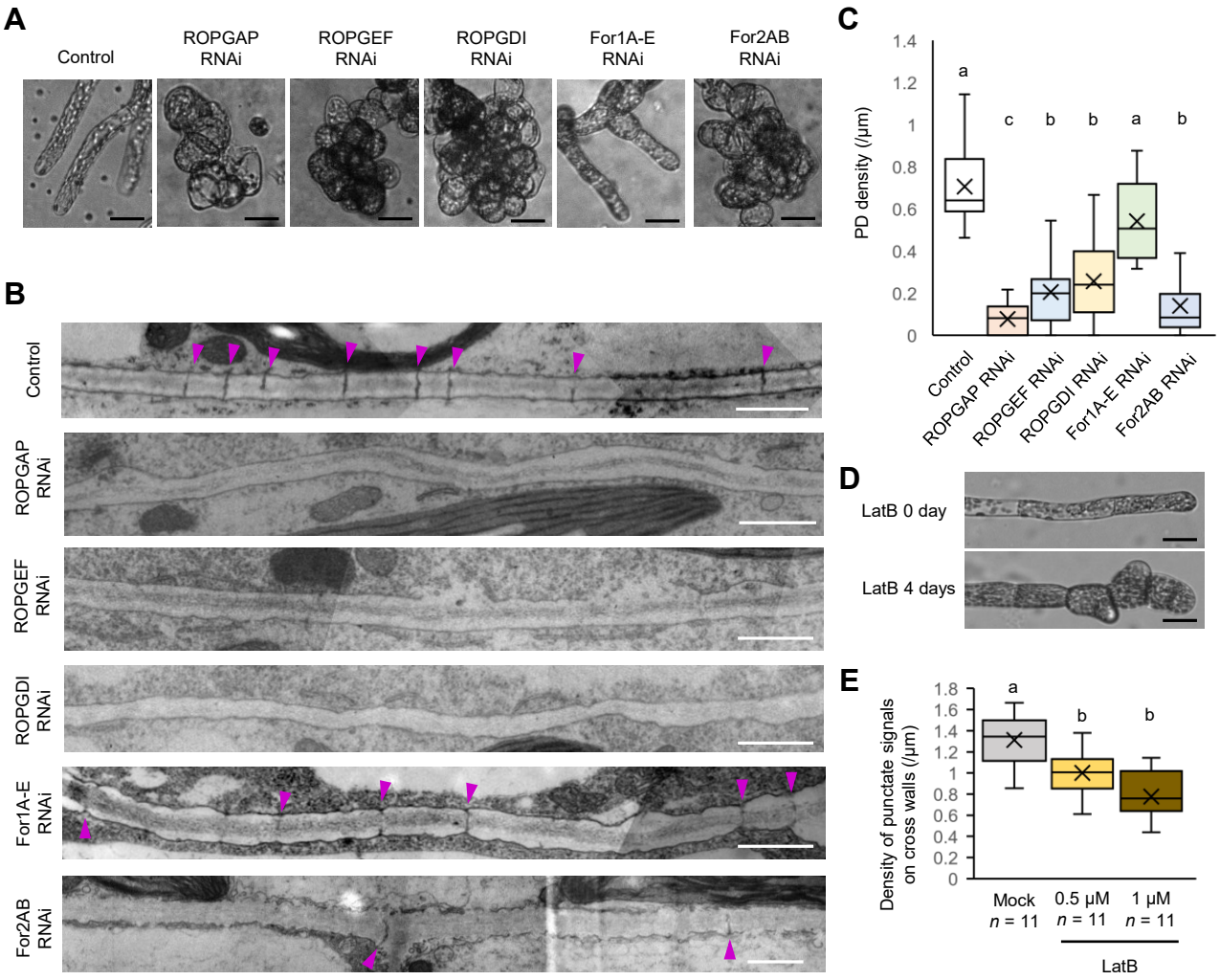

Chapter 3; Figure 4

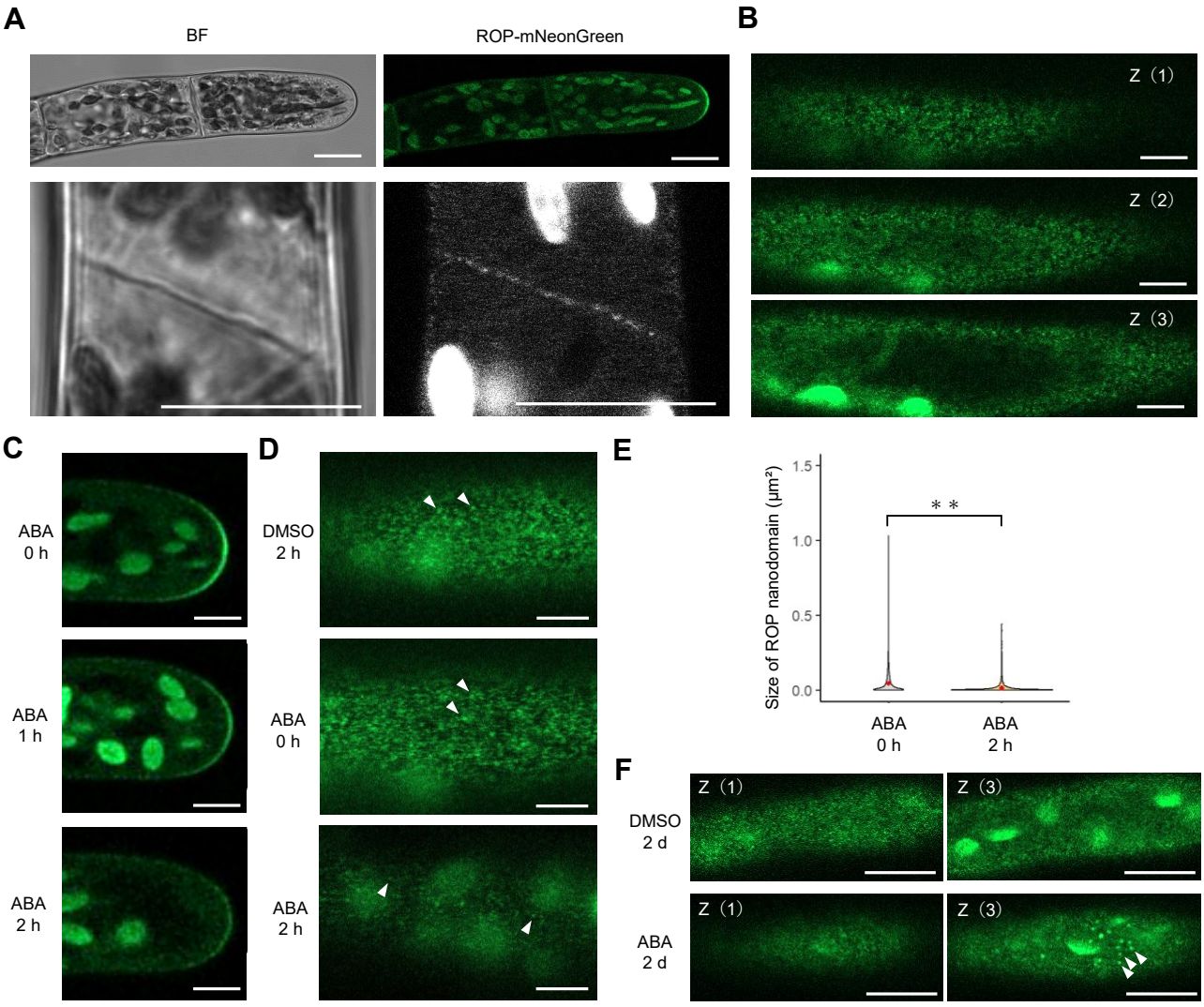

Chapter 3; Supplementary Figure S1

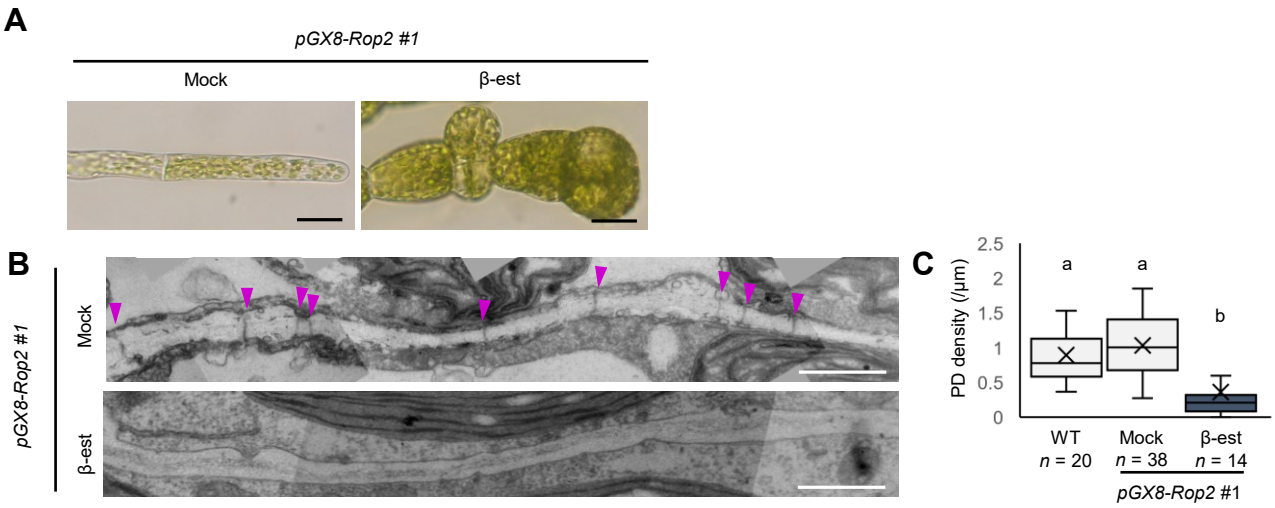

Chapter 3; Supplementary Figure S2

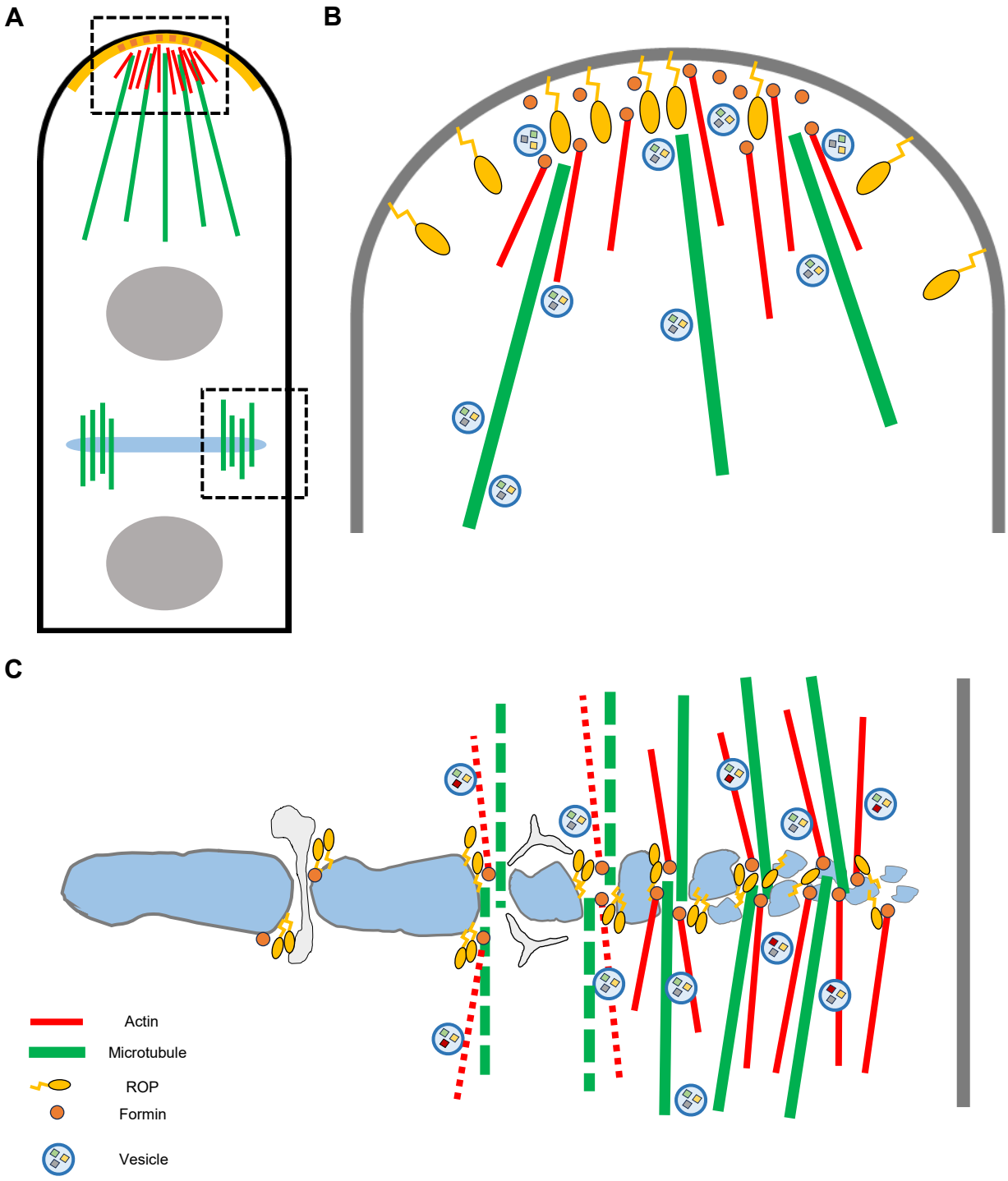

Chapter 3; Supplementary Figure S3